

Review

Heat Transfer Enhancement of Nanofluids with Non-Spherical Nanoparticles: A Review

Xiaoyin Li ^{1,2}, Fangyang Yuan ^{1,2,*}, Wenma Tian ^{1,2}, Chenlong Dai ^{1,2}, Xinjun Yang ^{1,2}, Dongxiang Wang ^{1,2}, Jiyun Du ^{1,2}, Wei Yu ^{1,2} and Huixin Yuan ³

- ¹ Jiangsu Key Laboratory of Advanced Food Manufacturing Equipment and Technology, Jiangnan University, Wuxi 214122, China; 6200809017@stu.jiangnan.edu.cn (X.L.); 6210810102@stu.jiangnan.edu.cn (W.T.); 6210810042@stu.jiangnan.edu.cn (C.D.); xinjun_yang@jiangnan.edu.cn (X.Y.); dxwang@jiangnan.edu.cn (D.W.); jiyundu@jiangnan.edu.cn (J.D.); yuwei0301@jiangnan.edu.cn (W.Y.)
- ² School of Mechanical Engineering, Jiangnan University, Wuxi 214122, China
- ³ Department of Mechanical Engineering, Taihu University of Wuxi, Wuxi 214063, China; yhx@cczu.edu.cn
- * Correspondence: fyyuan@jiangnan.edu.cn

Abstract: This article reviews the heat transfer enhancement of nanofluids with non-spherical nanoparticles. We divided the non-spherical nanoparticles suspended in nanofluids into three categories based on the dimension of geometric particle structure. Based on the measured data in experimental studies, we then evaluated the shape effect of non-spherical nanoparticles on thermal conductivity and convective heat transfer enhancement of nanofluids. Recent studies explored the numerical predictions and related heat transfer mechanisms. Due to large aspect ratios, thermal conductivity is abnormally enhanced only for nanofluids with carbon nanotubes/nanofibers/nanowires. The approximate enhancement effect exerted by three types of non-spherical nanoparticles on thermal conductivity was 4.5:2.5:1. Thermal conductivity enhancement per concentration was larger for nanorods/ellipsoids with small aspect ratios. The convective heat transfer coefficient was increased by suspending non-spherical nanoparticles in the base fluid. Consequently, no significant thermo-hydraulic performance was discovered for convective heat transfer of non-spherical nanoparticle nanofluid flow, specifically for turbulent flows, due to increased pumping power. However, the temperature and particle concentration effect on convective heat transfer remains unclear. In addition, no perfect model for predicting the thermal conductivity and convective heat transfer of non-spherical nanoparticle nanofluids has been reported.

Keywords: nanofluids; non-spherical nanoparticles; heat transfer enhancement; thermal conductivity; convective heat transfer



Citation: Li, X.; Yuan, F.; Tian, W.; Dai, C.; Yang, X.; Wang, D.; Du, J.; Yu, W.; Yuan, H. Heat Transfer Enhancement of Nanofluids with Non-Spherical Nanoparticles: A Review. *Appl. Sci.* **2022**, *12*, 4767. <https://doi.org/10.3390/app12094767>

Academic Editor: Luis Lugo

Received: 21 April 2022

Accepted: 6 May 2022

Published: 9 May 2022

Publisher's Note: MDPI stays neutral with regard to jurisdictional claims in published maps and institutional affiliations.



Copyright: © 2022 by the authors. Licensee MDPI, Basel, Switzerland. This article is an open access article distributed under the terms and conditions of the Creative Commons Attribution (CC BY) license (<https://creativecommons.org/licenses/by/4.0/>).

1. Introduction

Studies on heat transfer enhancement of nanofluids have largely matured over the past decade. Since Choi and Eastman [1] introduced the concept of “nanofluids,” which are fluids with suspended nanoparticles, scholars have reported significant heat transfer enhancement of nanofluids with low particle loadings. In addition, the suspension is stable and induces a small amount of pumping power compared to the base fluid [2]. Therefore, nanofluids are considered the next generation of a heat transfer medium that will be extensively applied in advanced heating or cooling technology.

Due to the complexity of the nanofluid flow transport, the mechanism underlying the excellent heat transfer performance of nanofluids is poorly understood. The bulk medium shows rheological behavior after the nanoparticles are dispersed in the base fluid [3,4]. Murshed and Estellé reviewed the viscosity of nanofluids with different types of nanoparticles or base fluids, particle concentration, shear rate, etc. [5]. However, they discovered scattered and inconsistent literature data from different researchers. Moreover, the conventional and proposed empirical models could not effectively predict the viscosity

of nanofluids containing non-spherical nanoparticles. Similar scenarios have been reported in heat transfer characteristics of nanofluids. First, there is a substantial variance in the thermal conductivity of nanofluids measured in the literature [6,7].

On the other hand, the convective heat transfer coefficient or Nusselt number provided in literature for nanofluid flow is different and inconsistent [8,9]. The contributing factors for nanofluids' heat transfer characteristics multiply, resulting in nonlinear correlations. Therefore, reviewing the results from previous studies is essential to identify research gaps.

Heat transfer enhancement of nanofluids is influenced by several factors, including particle material, size, shape, concentration, type of base fluid, the temperature of bulk fluid, etc. For convective heat transfer (CHT), the flow parameters and thermal boundary conditions promote nanofluids flow. Most of the previous studies focused on the importance of fluid type and particle concentration. Based on the effective medium theory, the enhancement of nanofluids heat transfer increases with the concentration and the thermal conductivity of the particle material. Nonetheless, the effect of particle shape and size distribution was partially reported and considered a constant in experiments or theoretical studies. The nanoparticles prepared for experiments in laboratories or applications in industries are polydisperse. The shape and size of particles vary around the nominal value given by nanomaterial producers.

Moreover, most studies on nanofluids' heat transfer enhancement are based on bulk fluid with spherical nanoparticles. With nanotechnology, more nanoparticles with different shapes can be industrially developed. In recent years, several experimental, theoretical, and numerical studies reported that particle shape modulates the CHT characteristic of nanofluids [10,11]. Nanoparticles with shapes such as cylinders, bricks, blades, and platelets have been discussed (Figure 1). Furthermore, a theoretical and numerical investigation of heat transfer enhancement of nanofluids containing non-spherical nanoparticles (NSN nanofluids) has recently gained a premium [12,13]. Therefore, it is essential to review the existing research on the importance of the particle shape effect on the nanofluid application in heat transfer enhancement.

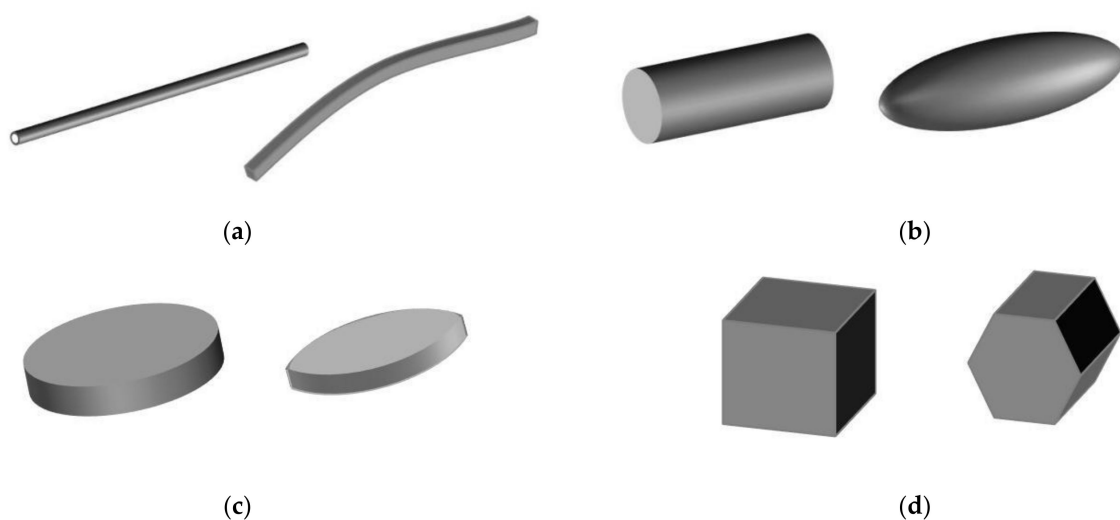


Figure 1. Shapes of non-spherical nanoparticles used in nanofluids. (a) CNTs/nanofibers/nanowires; (b) rods/cylinder/ellipsoids; (c) platelets/blades; (d) bricks/diamonds/polygons.

This article reviews research findings and the development of the heat transfer enhancement of NSN nanofluids. We collect and analyze thermal conductivity enhancement (TCE) measured in experiments based on NSN nanofluids. This work also summarizes the classical and recently proposed thermal conductivity models for NSN nanofluids and the related mechanisms. Further, we evaluate the experimental data in studies on CHT of NSN nanofluids. Finally, we present conclusions on the basic theory and numerical predictions for NSN nanofluids fluid with CHT.

2. Thermal Conductivity of NSN Nanofluids

Thermal energy transfer occurs through conduction, convection, or radiation [14]. Considering that radiative energy transport is quite distinct from the first two mechanisms because it does not require a material medium, we primarily focus on conduction and convection behaviors. This section deals with the thermal conductivity of NSN nanofluids, whereas heat transfer via convection will be discussed in the next sections.

2.1. Experimental Data Evaluation

Thermal conductivity is an essential physical property of nanofluid conduction. Several studies have been performed to enhance nanofluids' thermal conductivity. For NSN nanofluids, Table 1 summarizes experimental studies on the thermal conductivity enhancement of NSN nanofluids. The experimental conditions vary in the nanofluid type, particle shape, size, volume fraction, and temperature. Distilled water (DW) was commonly used for aqueous nanofluids, and oil was used as the base fluid. Most of the experiments were performed by transient hotwire technology in the lab. The insulation treatment of the sensor and control of surfactant is significantly essential [15]. As shown in the table, all of the experimental results showed the thermal conductivities of nanofluids were enhanced after nanoparticles were suspended in the base fluid. Results showed that the thermal conductivity of nanofluids increases as the particle loading grows. However, not all data demonstrated the abnormal thermal conductivity capacity of nanofluids with non-spherical nanoparticles. Figure 2 presents the experimental data in Table 1 to compare the TCEs of different NSN nanofluids at room temperature. Considering the continuous variation in TCE with temperature, data were obtained by interpolation within the temperature range.

The shapes of non-spherical nanoparticles used in studies can be divided into three categories based on the dimensionality of particle geometry [13,16]. Carbon nanotubes (CNTs), nanofibers, and nanowires are approximated as one-dimensional elongated particles with a large aspect ratio (AR, ratio of length to diameter of particles). Their cross-section size is in the nanometer range. However, the length is several microns or even longer. In addition, their bending states differ due to different materials.

Nevertheless, these particles with large aspect ratios are easily intertwined, inducing a network effect [17]. Their rheological characteristics are significantly apparent. Rod-like and ellipsoidal particles are categorized as two-dimensional nanomaterials with a moderate aspect ratio of 1 to 10. If the length is much less than the cross-sectional diameter, the particle usually appears as a disk shaped like a platelet or a blade, as shown in Figure 1c. Additional types of particles with arbitrary shapes such as bricks, diamonds, and other polygonal shapes are three-dimensional classes. From the average slope of the three zones, the approximate enhancement effect by three types of non-spherical nanoparticles on thermal conductivity is 4.5:2.5:1. The thermal conductivity characteristics of three types of NSN nanofluids are discussed.

2.1.1. CNTs/Nanofibers/Nanowires

CNTs are the most popular suspension medium for nanofluids since they display an average thermal conductivity of 4000 W/(m·K), which is higher than that of other nanoparticles [18]. Many articles and reviews [19–21] focused on nanofluids with CNTs, and only representative work is listed in Table 1. The type of nanofluid with elongated nanoparticles shows excellent performance in TCE due to the large size and aspect ratio of CNTs, which are hundreds of nanometers in diameter and at least tens of microns in length [15,22]. Nevertheless, the addition of large-aspect-ratio particles into a base fluid could significantly increase viscosity compared to the continuous phase [23]. Moreover, CNTs, another nanofibrous polymer [15], and nanowires [24] entangle with each other, which could cause a complex particle morphology and heat transfer properties in different experiments. Ali et al. [21] recently reviewed the thermal conductivity of commonly used particles and base fluids for fabricating nanofluids and showed that carbon-based nanofluids hold superior thermal features to those prepared by metal oxides and metals.

Figure 2 displays a number of points showing the enhancement of heat conduction in varying ranges. Maheshwary et al. [25,26] reported doubled thermal conductivities after suspending 2.5 wt.% metal oxide nanoparticles. They compared three nanofluids with cubic, nanorod, and spherical nanoparticles; they concluded that cubic particles displayed the best performance. Their abnormal results are significantly more excellent than others represented in Figure 2a. Thus, they are not plotted in the figure. The TCE shows two distinct trends that the black dotted line can distinguish in the figure in a wide range of volume fractions. Several studies reported abnormal TCE within 1% particle loading. Xie et al. [27,28] prepared nanowires with high aspect ratios (25 for Ag and approximately 82 for CuO nanowires) and measured an intriguingly high thermal conductivity increment at low volume fractions.

In contrast, the TCE for nanofluid containing CuO nanospheres remains low. Therefore, thermal conductivities for NSN nanofluids can be much higher than those of nanofluids containing spherical nanoparticles. The study also showed that the TCE linearly increases with the volume fraction when the nanowire volume fraction is lower than 1%, and the authors discovered that their data effectively conforms to the Hamilton–Crosser (H-C) model. Intriguingly, Carbajal-Valdéz et al. [29] reported a TCE of 20.8% by suspending only 0.0174% Ag nanowires, which shows a performance approximately 20 times better than the results of Gu et al. [24]. Overall, nanofluids with CNTs/nanofibers/nanowires demonstrate the best performance in different types of nanofluids. Specifically, nanofluids prepared with Ag nanowires at low concentrations show abnormal TCE.

2.1.2. Nanorods/Ellipsoids

Nanofluids containing cylindrical nanoparticles are another type of suspension commonly used in research [2,10,30,31]. Notably, nanoparticles in cylindrical shape are referred to as nanorods with stiffness and finite length. These nanomaterials are synthesized from metals or semiconducting materials and cannot bend. The cross-section of particles is circular and nanosized, with a moderate aspect ratio range of around 5 [32]. Yang and Han [31] documented that nanofluids containing cylindrical nanoparticles with such an aspect ratio could show different behaviors.

In Figure 2, the findings reported by Murshed et al. [2] and Zhu et al. [33] are quite similar when particle loading ranges from 2% to 5%. The aspect ratios of used nanorods are approximately 4 and 6.25, and the materials include TiO₂ and CuO, respectively. Timofeeva et al. suspended aluminum oxide (Al₂O₃) nanoparticles of four different shapes [34] in DW and EG mixed 50/50 by volume to assess the particle shape effect on thermal conductivity of nanofluids. The nanoparticles supported by a company have the shapes of rods, bricks, platelets, and blades, with different sizes and aspect ratios. The data measured in experiments illustrated that nanofluids containing cylindrical nanoparticles exhibit the best heat conductivity performance. They found that particle shape and interfacial layer contribute to the particle volume fraction thermal conductivity of nanoparticle suspensions. The predictions of the classical H-C model are higher than the measured TCE for particles with blade and platelet shapes.

Other studies [10,31,35] measured similar values of TCE, which are approximately half of the TCE reported by Murshed et al. [2] and Zhu et al. [33]. Chen et al. [3] prepared aqueous nanofluids containing CNTs with an aspect ratio of 10, closer to rod-like. Nithiyantham et al. [36] suspended rod-like Al₂O₃ nanoparticles into molten salt to prepare nanofluids and discovered approximately 10% TCE in the liquid state. The particle shapes discussed above have an aspect ratio larger than 1. As shown in Figure 1, the nanofluid TCE is positively related to the particle concentration. To eliminate the effect of particle concentration to examine the shape effect, we defined the enhancement per concentration as the ratio of TCE and particle volume fraction. Figure 3 shows the enhancement per concentration as a function of aspect ratio at room temperature. Only a handful of studies have provided particle aspect ratios. Ag nanowire/CNT-based nanofluids made by Gu et al. [24] and Carbajal-Valdéz et al. [29] were not plotted due to the out-of-range values.

Nanoparticles agglomerate and form aggregates with a small aspect ratio; this explains why many studies have found enhanced heat transfer except for the concentration increment. With increasing AR, the enhancement per concentration increases; this implies that a non-spherical shape helps TCE. The reported data are near the diagonal (enhancement per concentration/AR = 1). Interestingly, the increase induced by the aspect ratio appears to be more apparent in the small-aspect-ratio region (AR < 10), which represents rod-like particles. TCE per concentration no longer increased with increasing AR for a tubular/wire-shaped dispersed phase with a large aspect ratio. This means that the enhancement of the network effect on heat transfer is limited. Jiang et al. [37] discovered that the effect of particle AR on TCE was more apparent for small particles.

2.1.3. Platelets/Blades/Bricks/Diamonds/Polygons

Platelet/blade-shaped particles have a large section area. The data plotted in Figure 2 reveal a relatively small TCE of this nanofluid type. Singh et al. [38] measured a TCE of approximately 29.51% at a high volume fraction of SiC–water nanofluid of 7%. Timofeeva et al. [34] compared the effects of the particle shapes of platelets, blades, and cylinders on TCE by eliminating the material and agglomeration effect. They discovered that although the sphericities of blades and platelets are larger than those of cylinders, the measured TCE of blades and platelets is smaller than that of cylinders. The classical H-C model considers the sphericity of non-spherical particles and cannot estimate the shape effect on the TCE of nanofluids. Similar results were obtained by Kim et al. [39] in a comparison of platelet-, brick-, and blade-shaped particles.

Torii and Yang [40] and Xie et al. [41] investigated nanofluids with diamond-like particle shapes; however, these particles are treated as spheres. Their findings showed that TCE linearly increases with particle volume fraction. Ferrouillat et al. [42] tested nanofluids with polygonal nanoparticles and discovered a slight difference between nanofluids and base fluid. Notably, particle sizes differ among these studies, which could also influence the TCE. Enhancement per concentration as a function of particle size at room temperature is illustrated in Figure 4. Experimental data reported in Table 1 are plotted, except for those of Maheshwary et al. [25,26], whose findings were two orders of magnitude higher than other results. As shown in Figure 4, most of the enhancement per concentration is smaller than 10, indicating a relatively weak shape effect of these particles on TCE. From the data of diamond and platelet particles, the enhancement per concentration increases with increasing particle size.

Nonetheless, the materials of nanoparticles as additives dispersed in the nanofluids are different, and studies demonstrated a different behavior in particle size effect [43]. Tahmooressi et al. [44] recently argued that there is insufficient evidence that smaller nanoparticles increase ETC more than larger nanoparticles. Heat conductivities of nanofluids with blade- or brick-shaped nanoparticles measured by Kim et al. [39] and Timofeeva et al. [34] are close and lower than those of other shapes due to the sphericity of bricks being close to 1.

Table 1. Summary of experiments data for heat conductivity of NSN nanofluids.

Authors	Nanofluid Type	Particle Shape and Size (nm as Default)	Volume Fraction ϕ (Vol. as Default)	Temperature	Maximum TCE
Xie et al. [30]	SiC–water/EG	Cylindrical 600 (<i>d</i>)	<4.2%	4 °C	22.9%
Xie et al. [22]	CNTs–DE/EG/DW	Nanotube 15 (<i>d</i>) × 30 mm (<i>l</i>)	1%	-	19.6% in DE, 12.7% in EG, 7.0% in DW
Assael et al. [45]	CNTs–water	Nanotube, 30 to 250 (<i>d</i>), <i>l</i> > 70,000	0.6%	Room	38%
Murshed et al. [2]	TiO ₂ –water	Nanorod 10 (<i>d</i>) × 40 (<i>l</i>)	<5%	Room	33%
Yang and Han [31]	Bi ₂ Te ₃ –perfluoro- <i>n</i> -hexane	Nanorod 20 (<i>d</i>) × 170 (<i>l</i>)	0.8%	3–50 °C	7.7% at 3 °C, 6.3% at 50 °C
Yang and Han [31]	Bi ₂ Te ₃ –hexadecane oil	Nanorod 20 (<i>d</i>) × 170 (<i>l</i>)	0.8%	20–50 °C	6.1% at 20 °C, 3.9% at 50 °C

Table 1. Cont.

Authors	Nanofluid Type	Particle Shape and Size (nm as Default)	Volume Fraction ϕ (Vol. as Default)	Temperature	Maximum TCE
Zhang et al. [15]	CNTs–water	Nanofiber 150 (d) \times 10,000 (l)	0.1–0.89%	23 °C	40%
Zhu et al. [33]	CuO–water	Nanorod 30–50 (d) \times 200–300 (l)	0.1–10%	Room	18% at $\phi = 1\%$, 28% at $\phi = 3\%$, 31% at $\phi = 5\%$
Chen et al. [3]	TiO ₂ –water	Nanorod 10 (d) \times 100 (l)	0.12, 0.24, and 0.60%	20–40 °C	5.38%
Singh et al. [38]	SiC–water	Platelet 170 (d)	<4%	Room	~29.51%
Timofeeva et al. [34]	Al ₂ O ₃ –EG and water (50/50)	Platelet 16 (d) \times 3 (l)	<7%	21 °C	18% at $\phi = 7\%$
Timofeeva et al. [34]	Al ₂ O ₃ –EG and water (50/50)	Blade36 (d) \times 6 (l)	<7%	21 °C	18% at $\phi = 7\%$
Timofeeva et al. [34]	Al ₂ O ₃ –EG and water (50/50)	Cylinder 8 (d) \times 64 (l)	<8.5%	21 °C	35% at $\phi = 8.5\%$
Timofeeva et al. [34]	Al ₂ O ₃ –EG and water (50/50)	Brick 54 (l)	<7%	21 °C	25% at $\phi = 7\%$
Torii and Yang [40]	nanodiamonds–water	Diamond 10 (d)	<5%	-	16%
Xie et al. [41]	nanodiamonds–water/EG	Diamond 30–50 (d)	<2%	10–60 °C	18%
Yu et al. [10]	Al ₂ O ₃ –PAO	Nanorod 7 (d) \times 85 (l)	<1.3%	25 °C	12% at $\phi = 1.3\%$
Nasiri et al. [46]	SWNT/SWNT/ FWNT/MWNT–water	-	0.25 wt.%	15–40 °C	13%, 16%, 21%
Gu et al. [24]	CNTs–water	Nanofiber 10–15 (d) \times 10–20 μ m (l)	0.2%	25 °C	3.7%
Gu et al. [24]	Ag–water	Nanowire 60 (d) \times 20,000–30,000 (l)	0.2%	25 °C	12.1%
Gu et al. [24]	Cu–water	Nanowire 100–200 (d) \times 800–6000 (l)	0.2%	25 °C	2.8%
Ferrouillat et al. [42]	SiO ₂ –water	Banana-like	0.82%	20–70 °C	2% at 70 °C
Ferrouillat et al. [42]	ZnO–water	Nanorod	0.93%	20–70 °C	1% at 70 °C
Fang et al. [47]	Ag–EG	Nanowire 100 (d) \times 50,000 (l) Platelet, 300–400 (d) \times 30–40 (l)	0.1%	10–30 °C	15.6% 5.3%
Jeong et al. [48]	ZnO–water	Nanorod, 150–370 (d) Platelets, 15 (d) \times 5 (l)	0.5–5%	Room	19.8% 23%
Kim et al. [39]	Al ₂ O ₃ –water	Blades, 15 (l) \times 8 (w) \times 5 (h) Bricks, 40 (d) \times 40 (l) \times 20 (l)	0.3–7%	20–80 °C	16% 28%
Farbod et al. [49]	CuO–engine oil	Nanorod	<6 wt.%	25 °C	8.3%
8.3%	TiO ₂ –water	Cubic, 87.21 (d) Nanorod, 8.27 (d) \times 92.47 (l)	<2.5 wt.%	27–87 °C	169% 96%
Zhang et al. [28]	Ag–EG	Nanowire 40 (d) \times 1000 (l)	0.46%	25 °C	13.42%
			0.15%		13.42%
			0.3%		23.15%
Zhu et al. [27]	CuO–dimethicone	Nanowire 30–80 (d) \times 3500–5500 (l)	0.45% 0.6% 0.75%	25 °C	36.98% 47.67% 60.78%
		Cube, 68.4 (l)			16.98%
Shah et al. [50]	CuO–EG and DW (70/30)	Brick, AR = 1.07 Polygonal, AR = 1.57 Nanorod, AR = 5.84	0.3%	30–80 °C	22.30% 29.50% 33.17%
Carbajal et al. [29]	Ag–water	Nanowire 96 (d) \times 40,000 (l)	0.0174%	Room	20.8%
Maheshwary et al. [25]	CuO–water	Cubic, Nanorod	2.5 wt.%	30 °C	72.49% 48.81%
Maheshwary et al. [25]	MgO–water	Cubic, Nanorod	2.5 wt.%	30 °C	110.96% 72.57%
Maheshwary et al. [25]	TiO ₂ –water	Cubic Nanorod	2.5 wt.%	30 °C	148.46% 115.55%
Maheshwary et al. [25]	ZrO ₂ –water	Cubic, Nanorod	2.5 wt.%	30 °C	164.01% 135.36%
Maheshwary et al. [25]	Al ₂ O ₃ –water	Cubic, Nanorod	2.5 wt.%	30 °C	209.70% 173.31%
Nithiyanantham et al. [36]	Al ₂ O ₃ –molten salt	Nanorod, 3–7 (d) \times 30–70 (l)	1 wt.%	50–200 °C	10.08%

Table 1. Cont.

Authors	Nanofluid Type	Particle Shape and Size (nm as Default)	Volume Fraction ϕ (Vol. as Default)	Temperature	Maximum TCE
Cui et al. [35]	TiO ₂ -water	Ellipsoidal, 20 (<i>d</i>) × 30 (<i>l</i>)	0.5–4%	20–60 °C	20.58%
		Nanorod, 15 (<i>d</i>) × 35 (<i>l</i>)			20.63%
		Sheet, 5 (<i>w</i>) × 70 (<i>l</i>) × 70 (<i>h</i>)			23.43%
Ni et al. [51]	Cu ₂ O-water	Nanowire, 2–3 (<i>d</i>)	-	30–80 °C	66.8%

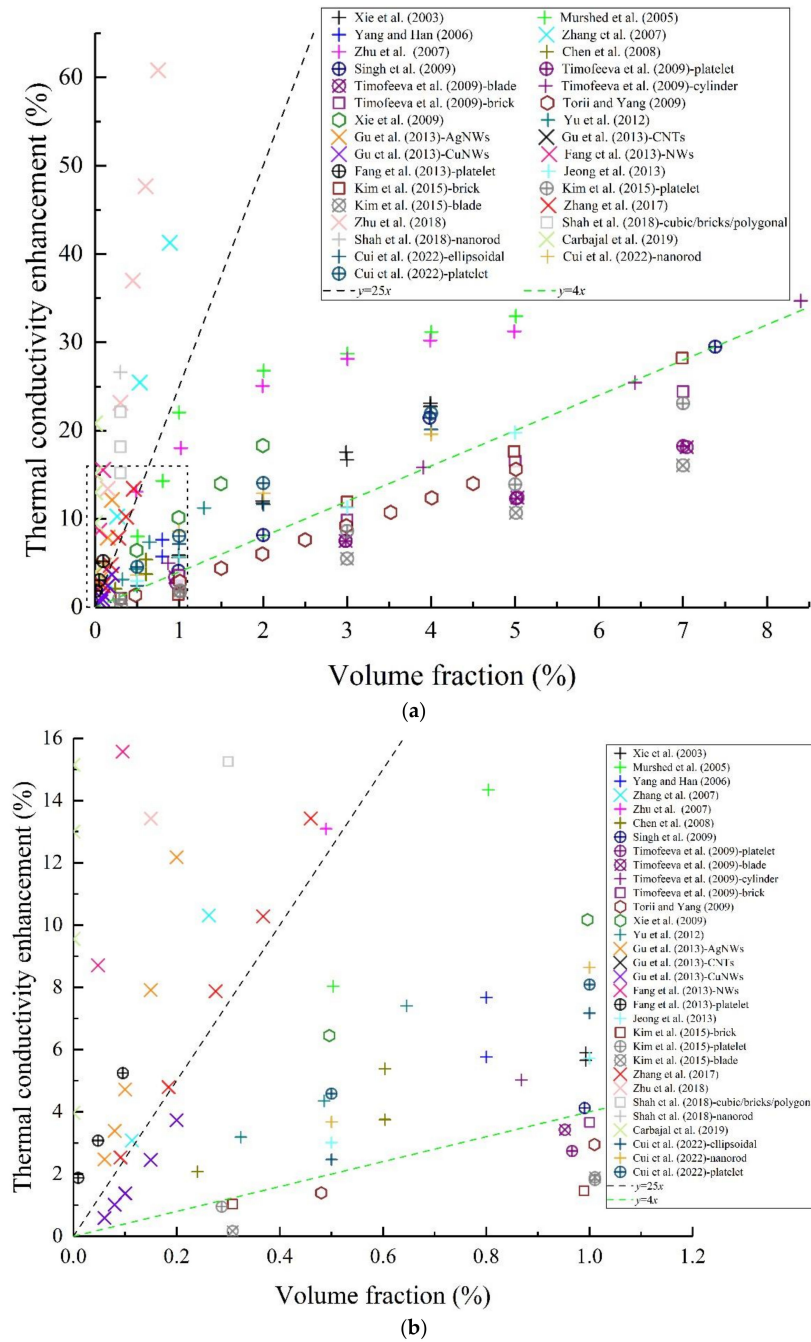


Figure 2. Collection of experimental data for TCE of NSN nanofluids at room temperature (×: CNTs/nanofibers/nanowires; +: nanorods/cylinders/ellipsoids; ⊕: platelets; ⊗: blades; □: bricks; ⬡: diamonds). (a) Full range. (b) Enlarged low-volume-fraction region (volume fraction < 1.2%, TCE < 16%) [2,3,10,15,22,24,27–29,31,33–35,38–41,47,48,50].

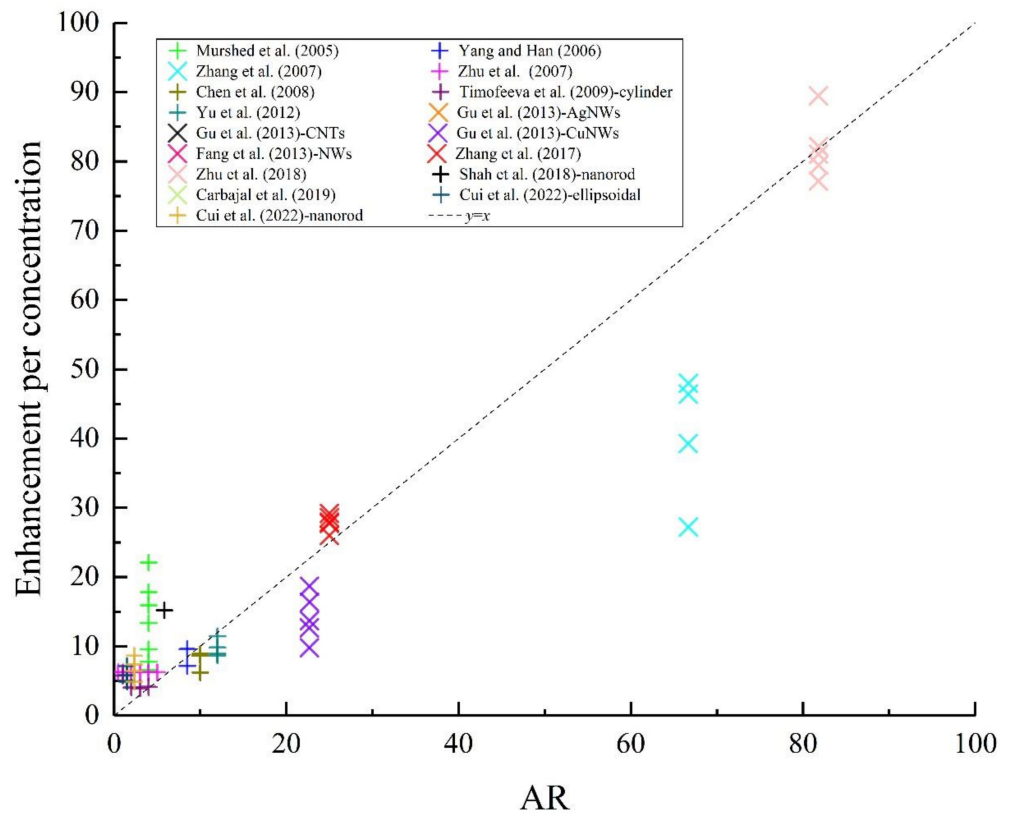


Figure 3. Enhancement per concentration as a function of aspect ratio at room temperature [2,3,10,15,24,27–29,31,33–35,47,50].

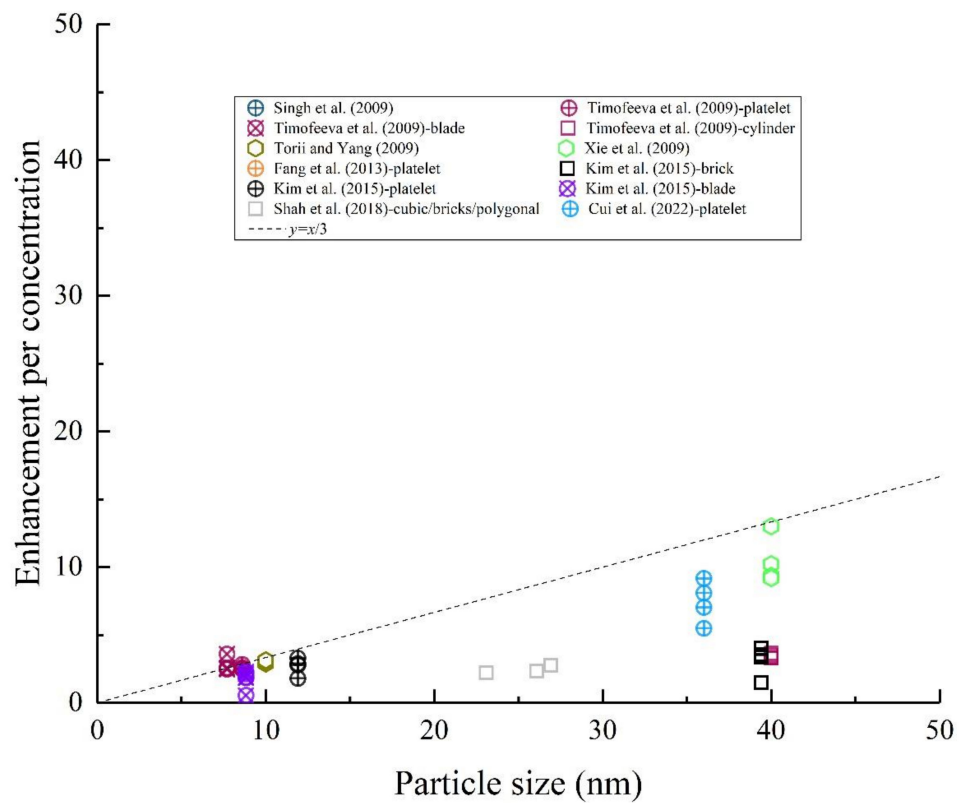


Figure 4. Enhancement per concentration as a function of particle size at room temperature [34,35,38–41,47,50].

2.2. Numerical Predictions and Mechanism Discussion

Effective heat conductivity (EHC) k is often used to describe the bulk ability of thermal conductivity. For suspensions with spherical particles, Maxwell [52] first presented the classical EHC model:

$$k_{nf} = k_f \left[\frac{(k_p + 2k_f) + 2\phi(k_f - k_p)}{(k_p + 2k_f) - \phi(k_f - k_p)} \right] \quad (1)$$

The formula is derived from spherical particles, but recent studies have found that it is also effective for diluting Newtonian nanofluids [17]. Based on the Maxwell model, Hamilton and Crosser [53] presented the model for suspensions with non-spherical particles:

$$k_{nf} = k_f \left[\frac{k_p + (n-1)k_f - (n-1)(k_p - k_f)\phi}{k_p + (n-1)k_f + (k_p - k_f)\phi} \right] \quad (2)$$

where n is the shape factor, and $n = 3/s_i$. s_i is the sphericity, which equals 3 for spherical particles. The data listed in Table 1 indicate that the EHC for nanofluids is influenced by particle shape and materials, particle loading, and pH. Wang et al. [54] established a model for nanoparticle aggregates by combining the effective medium approximation and the fractal theory. Nonetheless, the fractal dimension or shape factor index could not provide particle shape characteristics and the interaction with base fluids. Therefore, there is no perfect model to predict the thermal conductivity of various nanofluids accurately. Table 2 lists several popular models and numerical studies for EHC of NSN nanofluids. Nanofluids with tube/wire/cylinder-shaped nanoparticles showed superior TCE. Thus, the models in the literature are primarily established to focus on this type of particle. Most of these models are based on the classical H-C model and modified based on the experimental data or by combining the characteristics of nanofluids.

2.2.1. Interfacial Layer Theory

Nanofluids are composites with particle additives [55]. The liquid atoms of the base fluid near a nanoparticle will be absorbed into the solid surface of the nanoparticle and form an absorption layer [56]. The interfacial layer between particles and base fluid has a remarkable effect on thermal conductivity. For non-spherical particles, the surface area of the interfacial layer is much larger than that of spherical particles, which can trigger a larger heat flux. Nan et al. [57] presented a model for CNT nanofluids considering the interfacial thermal barrier resistance and found a significant interface effect on TCE. Many models [58–60] were built by considering the interfacial layer effect. The benefit of this theory is that it considers the effect of particle morphology from the microscopic point of view. Chandrasekar et al. [61] proposed a model considering the interfacial layer thickness, particle shape, and Brownian motion. They attributed the anomalous TCE to the particle shape.

Timofeeva et al. [34] believed that TCE for NSN nanofluids depends on the competition between surface contact area (enhancement) and Kapitza resistance (weakening). The model predicted that TCE would be negative when sphericity is smaller than 0.6 for Al_2O_3 -EG/water (50/50) nanofluids. Yang et al. [62–64] developed several EHC models based on the anisotropy analysis of cylindrical nanoparticles. They summed axial and radial direction heat transfer flux of cylindrical nanoparticles whose orientation distribution is uniform. These models are built exquisitely and are challenging to use. The shape of nanoparticles was first incorporated into an AI-based model for thermal conductivity by Cui et al. [35]. The results of the developed CFFNN model revealed that the cylindrical shape of nanoparticles with a large aspect ratio could trigger a rapid heat flow along longer thermally conducting pathways without the need to cross an interparticle boundary or junction point; this is beneficial to the thermal energy transfer in the nanofluids.

2.2.2. Nanoparticle Aggregation

The aggregation of nanoparticles significantly affects the thermal conductivity of nanofluid [65]. Studies based on nanofluid with spherical nanoparticles revealed that high TCE could be caused by particle aggregation [66]. Primary nanoparticles appear to aggregate to form aggregates or clusters which are non-spherical, particularly with increasing concentration. Wang et al. [67] evaluated the nanofluid thermal conductivity by molecular dynamics (MD) simulation and found that the aggregates can be divided into compact aggregation and loose aggregation. The atoms in the nanolayer are mobilized and dynamically balanced, which could be the mechanism for the TCE of the nanofluid. Due to the significant computational workload, only six nanoparticles were involved. Then, they proposed a hybrid method of multi-particle collision dynamics (MPCD) and MD to increase nanoparticles in calculations [68,69]. The simulations involving 32 nanoparticles showed that the EHC of nanofluid linearly increases with the decrease in the fractal dimension of the nanoparticle aggregates. Lee et al. [70] compared the classical density functional theory (DFT) to Poisson–Boltzmann theory and found a good agreement with experiments on heat transfer for nanofluids.

2.2.3. Network Effect

Sastry et al. [71] constructed a model based on the thermal resistance network by considering the random CNT orientation and CNT–CNT interaction. Their model effectively agreed with experimental data by assuming that a CNT contacts only two neighboring CNTs. Subsequently, Koo et al. [72] improved the model by considering the excluded volume of cylindrical particles. The revised model describes the effect of particle diameter and aspect ratio of CNTs and CNFs on TCE. The alignment of CNTs and CNFs due to the long-range repulsion force decreases the excluded volume, nonlinearly increasing the convexity and concavity and linearly increasing the thermal conductivity with particle concentration. Tahmooressi et al. [44] recently simulated the TCE of nanofluid using the lattice Boltzmann method and discovered that the network effect promotes the enhancement of heat transfer. Their algorithm prevents nanoparticles from forming aggregations by defining a minimum proximity distance.

2.2.4. Rotational Diffusion and Micro Convection

Xue [73] presented the equivalent field factor for CNTs distributed randomly in the base fluid and constructed a model for CNT nanofluids based on the Maxwell theory. They took the CNT as a rotational elliptical particle with a large aspect ratio. Ebrahimi et al. [74,75] built a model by neglecting the micro convection at the surface of cylindrical particles because the Brownian motion is slow. In addition, the collision model for non-spherical particles is difficult to construct. Models with the Brownian effect are based on spherical particles [76,77]. Cui et al. [78] found that cylindrical nanoparticles have a larger surface area and more energetic atoms than spherical nanoparticles, resulting in a larger TCE. Moreover, the high-speed rotation of cylindrical nanoparticles accelerates micro convection in the base fluid due to the stirring effect.

Table 2. Typical models for TCE of NSN nanofluids.

Authors	Particle Shape	Models (k_{nf}/k_f as Default)	Remarks
Hamilton and Crosser [53]	Arbitrary	$\frac{k_p + (n-1)k_f - (n-1)(k_p - k_f)\phi}{k_p + (n-1)k_f + (k_p - k_f)\phi}$	Reduce to Maxwell model when $n = 3$
Yamada and Ota [79]	Cylinder	$\frac{k_p/k_f + K - K\phi(1 - k_p/k_f)}{k_p/k_f + K + \phi(1 - k_p/k_f)}$	Unit-cell model Consider the shape factor $K = 2\phi^{0.2}$ ($2l/d$) for cylindrical particles
Wang et al. [54]	Aggregates	$k_{eff} = (1 - \Phi) + 3\Phi \int_0^\infty \frac{\frac{k_{cl}(r)n(r)}{k_{cl}(r) + 2k_f} dr}{(1 - \Phi) + 3\Phi \int_0^\infty \frac{k_f n(r)}{k_{cl}(r) + 2k_f} dr}$	Combine the effective medium approximation and the fractal theory

Table 2. Cont.

Authors	Particle Shape	Models (k_{nf}/k_f as Default)	Remarks
Nan et al. [57]	CNTs	$\frac{3 + (\frac{2(k_{11}^c - k_f)}{k_{11}^c + k_f} + \frac{k_{33}^c}{k_f} - 1)\Phi}{3 - \frac{2(k_{11}^c - k_f)}{k_{11}^c + k_f}\Phi}$	Incorporating the interface thermal resistance
Xue [73]	CNTs	$\frac{1 - \Phi + 2\Phi \frac{k_p}{k_p - k_f} \ln \frac{k_p + k_f}{2k_f}}{1 - \Phi + 2\Phi \frac{k_f}{k_p - k_f} \ln \frac{k_p + k_f}{2k_f}}$	Based on Maxwell theory and considering the random CNT orientation distribution
Zhou and Gao [58]	Ellipsoid	Complicated	Differential effective medium theory
Ebrahimi et al. [74,75]	Cylinders/CNTs	$1 - \phi(1 + M') + \phi k_f(k_p + k_{layer}M') + \phi(1 + M')$	Interfacial layer theory
Sastry et al. [71]	CNTs	$\frac{a_f}{Pr_f(2a_p + \delta)} (0.35 + 0.56Re_f^{0.52}) Pr_f^{0.3}$	Brownian motion is neglected
Koo et al. [72]	CNTs/CNFs	$k_{eff} = \frac{\chi}{A} \left(\sum_{i=1}^N \frac{1}{\frac{k_{Eijid}A}{dx_i} + \frac{L_i}{\pi k_{CNT}d^2} + \frac{2}{Cd^2}} \right)^{-1}$	Assuming CNT contacts only two neighboring CNTs
Murshed et al. [59]	Cylinder	Based on model proposed by [71] $k_{eff} = ((k_p - k_{lr})\Phi_p k_{lr} [2\gamma_1^3 - \gamma^3 + 1] + (k_p + 2k_{lr}) \times \gamma_1^3 [\Phi_p \gamma^3 (k_{lr} - k_f) + k_f]) (\gamma_1^3 (k_p + 2k_{lr}) - (k_p - k_{lr})\Phi_p [\gamma_1^3 + \gamma^3 - 1])^{-1}$	Excluded volume concept Monte Carlo simulation
Timofeeva et al. [34]	Rods/bricks/ platelets/blades	Deduced in cylindrical coordinates	Consider particle shape and interfacial contributions
Chandrasekar et al. [61]	Arbitrary	$1 + (C_k^{shape} + C_k^{surface})\Phi$	Consider interfacial layer, particle shape, and Brownian motion
Cui et al. [78]	Cylinder	$k = \frac{k_s + (n-1)k + (n-1)(1+\beta)^3 \Phi(k_s - k)}{k_s + (n-1)k - (1+\beta)^3 \Phi(k_s - k)} + c \frac{\Phi(T - T_0)}{\mu k a^4}$	14.8% enhancement MD simulation based on the Green-Kubo formula
Jiang et al. [60]	CNTs	$k = \frac{1}{3V k_B T^2} \int_0^\infty \langle J(0)J(t) \rangle dt$	Interfacial layer theory
Yang et al. [64]	Cylinder	$\frac{k_p R(1+t/R - k_f/k_p) \ln(1+t/R)}{t k_f \ln[(1+t/R)k_p/k_f]} \beta_1 = 1 + t/R$ $k_{eff} = \frac{1}{\pi} \int_0^\pi (k_z^2 \sin^2 \varphi + k_x^2 \cos^2 \varphi)^{1/2} d\varphi$ $k_{eff2} = k_{eff2} \frac{2\pi r H}{2\pi r^2 + 2\pi r H} + k_{eff2} \frac{R_x}{R_z} \frac{2\pi r^2}{2\pi r^2 + 2\pi r H}$ $k_{eff2} = \frac{(k_p - k_{lr})\phi k_{lr} (\beta_1^2 - \beta^2 + 1) + (k_p + k_{lr})\beta_1^2 [\phi \beta^2 (k_{lr} - k_f) + k_f]}{\beta_1^2 (k_p + k_{lr}) - (k_p - k_{lr})\phi \beta_1 (\beta_1^2 + \beta^2 - 1)}$	Interfacial layer theory Consider end effect of cylinder
Yang et al. [62]	Cylinder	$k_{eff} = \frac{(H+2t)k_{eff,x} + (R+t)k_{eff,z}}{H+R+3t}$	Interfacial layer theory Anisotropy analysis
Yang and Xu [63]	Cylinder	$\frac{\overline{k_{pe} + k_{bf}(n-1) + (n+1)(\overline{k_{pe} - k_{bf}})(1+C)\phi}}{\overline{k_{pe} + k_{bf}(n-1) - (k_{pe} - k_{bf})(1+C)\phi}}$	Based on Hamilton-Crosser model Interfacial layer theory Anisotropy analysis
Wang et al. [67]	Aggregates (2–6 spheres)	Increases linearly with decrease in fractal dimension of aggregations	MD simulation
Du et al. [69]	Aggregates (6–32 spheres)	Increases linearly with decrease in fractal dimension of aggregations	Interfacial layer effect MPCD-MD simulation
Tahmooressi et al. [44]	Cylinder	$k_{eff} = \frac{L \int q dA}{\Delta T \int dA}$	Interfacial layer effect
Cui et al. [35]	Arbitrary	-	Lattice Boltzmann method CFNN model Artificial intelligence estimation

3. Convective Heat Transfer of NSN Nanofluids

Convective heat transport occurs when the bulk motion of nanofluids transports energy. The migration of suspended nanoparticles is induced by fluid hydrodynamics and thermodynamics. Furthermore, the relative motion between particles and a fluid affects the hydrodynamics and thermodynamics of the fluid. The complex interaction between discrete and continuous phases shows differences under different particle morphologies and surface treatments, flow structures, and heat transfer conditions. In this section, the experimental and numerical studies of NSN nanofluids are reviewed. The pool boiling heat transfer studies are not discussed since they have been exhaustively covered in the

literature [8,80–82]. In addition, CHT based on hybrid nanofluids is not included; the related studies have been reviewed by Vallejo et al. [83]. Several recent studies have shown that hybrid nanofluids have significant potential as a coolant in solar cells [84,85].

3.1. Experimental Data Evaluation

The Nusselt number is used to evaluate the ratio of CHT across the boundary. A more significant Nusselt number corresponds to more active convection. The dimensionless local Nusselt number in the channel is defined as:

$$\text{Nu} = \frac{h_{nf}D}{k_{nf}} \quad (3)$$

where the CHT coefficient is:

$$h_{nf} = \frac{q}{T_w - T_b} \quad (4)$$

where T_w is the wall temperature, T_b is the bulk temperature, and q is the heat flux. Flow loop experiments measure the parameters in Equation (4). A test section is set in a fully developed region with a straight or curved pipe/microchannel and a square or circular cross-section. In addition, it includes boundary layer flow, cavity flow [86,87], impinging jets, peristaltic flow, and flow in heat exchangers [12]. It can be divided into forced convection heat transfer or natural convection heat transfer. Based on the Reynolds number ($\text{Re} = u_0 L/\nu_{nf}$), the flow state is laminar, turbulent, or transitional flow [88]. Ghasemiasl et al. [89] analyzed the studies on the forced convection of nanofluids in circular and non-circular channels in terms of geometry, particles, methodology, and regime. Researchers evaluated the CHT features of nanofluids affected by different types of parameters and flow conditions. Table 3 presents the experimental and numerical studies for CHT of NSN nanofluids. The nanofluid type, particle shape and size, particle loading, and flow state are listed with CHT characteristics. Notably, all of the variations of the CHT coefficient or Nusselt number are typically nonlinear.

3.1.1. Different Analysis Parameters and Values

Research findings on nanofluid CHT document controversial arguments. The first is whether the CHT, not just the factor of TCE, is enhanced by suspending nanoparticles in the base fluid. The second is whether the thermohydraulic performance of nanofluids is better than that of the base fluid, relating to the efficacy of nanofluids for practical cooling applications. The different views could be caused by different analysis parameters. Studies perform the standard dimensionless analysis of CHT based on the Nusselt number and Reynolds number.

Nonetheless, researchers believe that the constant Reynolds number basis can be misleading since the net result for the constant Reynolds number comparison combines the nanofluid property effect and the flow velocity effect [90]. In the interpretation of nanofluid CHT, Buschmann et al. [17] argued that no anomalous phenomena are involved in the forced convection heat transfer of nanofluids. Their results show that heat transfer enhancement provided by nanofluids equals the increase in thermal conductivity of nanofluids compared to the base fluid. The CHT coefficient rather than the Nusselt number is more suitable to evaluate the intensity of the CHT of nanofluids. A notable exception was the experiments performed with non-spherical particles showing CHT enhancement of NSN nanofluids. Therefore, it is necessary to discuss the CHT of NSN nanofluids.

The magnitude of parameters selected for study is another point of view in nanofluid research. For experimental studies, the values are practical. However, for some numerical studies, the range of parameters could be beyond the scope of practical applications. Buongiorno [91] first evaluated different mechanisms in the convective transport in nanofluids. Myers et al. [92] claimed that the use of parameter values should represent an actual physical situation. Therefore, the experimental and numerical studies are discussed separately in the next section.

3.1.2. Thermohydraulic Performance Evaluation

Thermohydraulic performance is evaluated via a different criterion. As a heat transfer medium, a nanofluid should meet the appropriate guidelines before it can be applied. Yu et al. [93] evaluated their experimental data by different forms of figures of merit (FOMs) as follows:

- The ratio of CHT coefficient, $FOM_h = h_{nf}/h_b$;
- The ratio of the maximum overall temperature difference, $FOM_T = (T_{w,o} - T_{in})_{nf}/(T_{w,o} - T_{in})_b$;
- Cooling with minimum pumping power, $FOM_P = (c_p h/P)_{nf}/(c_p h/P)_b$;
- The relative ratio of heat transfer rate and pumping power, $FOM_Q = (q/P)_{nf}/(q/P)_b$.

The following criteria should be met: $FOM_h > 1$, $FOM_T < 1$, $FOM_P > 1$, and $FOM_Q > 1$. Research [94,95] has shown that the criteria for nanofluids with spherical particles are hardly met in tests. We sampled the CHT data of NSN nanofluids reported in the literature (Table 3). Ji et al. [96] used the relative thermal resistance to estimate the CHT performance of the nanofluid in an oscillating heat pipe; hence, the data are not shown. Nelson et al. [97] reported about 110 times viscosity of nanofluid with EG of 0.6% by weight in PAO, leading to a quite small FOM_P compared to others, which was excluded. The pumping power for other studies can be estimated based on Mansour et al. [98] for laminar and turbulent flows.

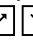

Most of the studies found an enhancement of the CHT coefficient if the FOM_h or FOM_T were used to evaluate the CHT varying with the Reynolds number. Nevertheless, suppose other performance evaluation criteria (PEC) are used. In that case, it can be found from the experimental data in Figure 5 that CHT was not far beyond the base fluid, with the majority of thermohydraulic FOM values being between 0.8 and 1.2. This is because the FOM_P and FOM_Q criteria were employed in most research, which combines heat transfer enhancement with an increase in pumping power. The heat capacity of nanofluids with low particle loading is close to that of the base fluid. The FOM_P for CNT nanofluids at $Re = 1200$ was a maximum of 1.536, which possibly meant that the data collection location was not fully developed. Ali et al. [99,100] tested the hydrodynamic performance of graphene nanoplatelet (GNP) nanofluids and discovered that the pumping power of nanofluids (caused by increased viscosity) was over twice that of the base fluid. Consequently, their results had the lowest FOM_P and FOM_Q values. Yu et al. [93] also found that different FOMs presented similar PEC for the same nanofluid.

Mikkola et al. [101] investigated the particle properties of CHT of nanofluids in the turbulent regime. Their experimental results based on oval-shaped Al_2O_3 nanoparticles demonstrated an increase of less than 5% in Nusselt number. Additionally, the CHT coefficient of nanofluids was roughly equal to that of base fluid when the volume concentration was lower than 1%. They used near-spherical particles. Furthermore, Ferrouillat et al. [42] and Wu et al. [102] investigated the CHT performance of nanofluids in turbulent regimes, and the PEC values were smaller than 1. Although the increased pumping power in turbulent flow is less than that of laminar flow, the thermohydraulic performance for NSN nanofluid in turbulent regimes is uneconomical. This also confirms why most recent studies are based on the laminar flow [89].

Yang et al. [23] and Contreras et al. [103] measured CHT coefficients of several types of nanofluids containing GNPs at different temperatures. The effect of operating temperature on CHT was unclear. In contrast, nanoparticle additives have a more significant impact on PEC. Table 3 shows that most tests are performed based on CNT or GNP nanofluids. These materials are easily accessible and commercially used in flow loop experiments. They have more significant thermal conductivity and specific surface area than those spherical particles. Bai et al. [104] also prepared GNP nanofluids with different particle loadings. The reported results revealed an increase in PEC with particle volume fraction.

Nonetheless, no similar findings were reported in other studies [93,101,102]. Similarly, no significant effect of shape factors on CHT was found, as shown in Figure 5. Additional data should be collected to confirm the CHT pattern of nanofluids under multiple factors.

Table 3. Experimental studies for CHT of NSN nanofluids.

Authors	Nanofluid	Particle Shape and Size (nm)	Particle Loading	Flow State	CHT Enhancement
Yang et al. [23]	Graphite–ATF graphite–oils	Plate-like, 1–2 μm (d) \times 20–40 (l)	2, 2.5 wt.%	Laminar, $5 < \text{Re} < 110$	$\text{Re}\uparrow, h\uparrow$ $\phi\uparrow, h\uparrow$ $T\uparrow, h\downarrow$ $\phi\uparrow, h\uparrow$ (significantly)
Ding et al. [105]	CNTs–water	-	<1 wt.%	Laminar, $800 < \text{Re} < 1200$	$x/D\uparrow, h\downarrow, \Delta h/h$   $\text{pH}\uparrow, h\downarrow$
Chen et al. [3]	Titanate NTs–water	Nanotube 10 (d) \times 100 (l)	0.5, 1.0 and 2.5 wt.%	Laminar, $1100 < \text{Re} < 2300$	$\phi\uparrow, h\uparrow$ $x/D\uparrow, h\downarrow$ $\text{Re}\uparrow, h\uparrow$
Nelson et al. [97]	Graphite–PAO	Plate-like, 20 μm (d) \times 100 (l)	0.3 and 0.6 wt.%	Laminar, $72 < \text{Re} < 365$	$\phi\uparrow, h\uparrow$
Ji et al. [96]	Al_2O_3 –EG and water (50/50)	Platelet, 9 (l) Blade, 60 (l) Cylinder, 80 (l) Brick, 40 (l)	0.3, 1, 3, and 5 vol.%	Oscillating heat pipe with input power 25–250 W	Heat transfer was enhanced significantly, nanofluids with cylindrical nanoparticles achieve the best performance
Yu et al. [10]	Al_2O_3 –PAO	Nanorod 7 (d) \times 85 (l)	0.65, 1.3 vol.%	Laminar, $150 < \text{Re} < 450$	$\text{Re}\uparrow, h\uparrow$ $\phi\uparrow, h\uparrow$ $x/D\uparrow, h\downarrow$
Ferrouillat et al. [42]	SiO_2 –water	Banana-like (nanorod)	2.28 vol.%	$200 < \text{Re} < 15,000$	Larger Nu for particles in banana shape than sphere in turbulent regime
Ferrouillat et al. [42]	ZnO–water	Polygonal/nanorod	0.82, 0.9 vol.%	$200 < \text{Re} < 15,000$	8% and 3% increase in Nu, respectively
Paul et al. [95]	Al_2O_3 –NEILs	Whisker	0.18, 0.36, 0.9 vol.%	-	Degradation of natural convection
Wu et al. [102]	CNTs–water	Nanotube 9.5 (d) \times 1500 (l)	<1 wt.%	-	Has no CHT enhancement
Arshad and Ali [100]	Graphene– water	Platelet, 5000–10,000 (d)	10 vol.%	$300 < \text{Re} < 1000$	$\text{Re}\uparrow, h\uparrow$ Pumping power increases as well
Mikkola et al. [101]	Al_2O_3 –water	Ellipsoid, 10 (d)	0.5, 1 vol.%	$1000 < \text{Re} < 11,000$	$\text{Re}\uparrow, h\uparrow, \text{Nu}\uparrow$ $\Phi/k\uparrow, h =$ enhancement < 5%
Contreras et al. [103]	Graphene–EG and water (50/50)	Platelet	0.01, 0.05, 1 vol.%		Thermohydraulic performance coefficient ≈ 1
Bai et al. [104]	Graphene oxide–DI	Platelet, 0.8–1.2 (h) \times 500–5000 (d)	0.02, 0.05, 0.075, 0.1 vol.%	150–800	$\phi\uparrow, \text{Nu ratio}\uparrow$ $\text{Re}\uparrow, \text{Nu ratio}\uparrow$

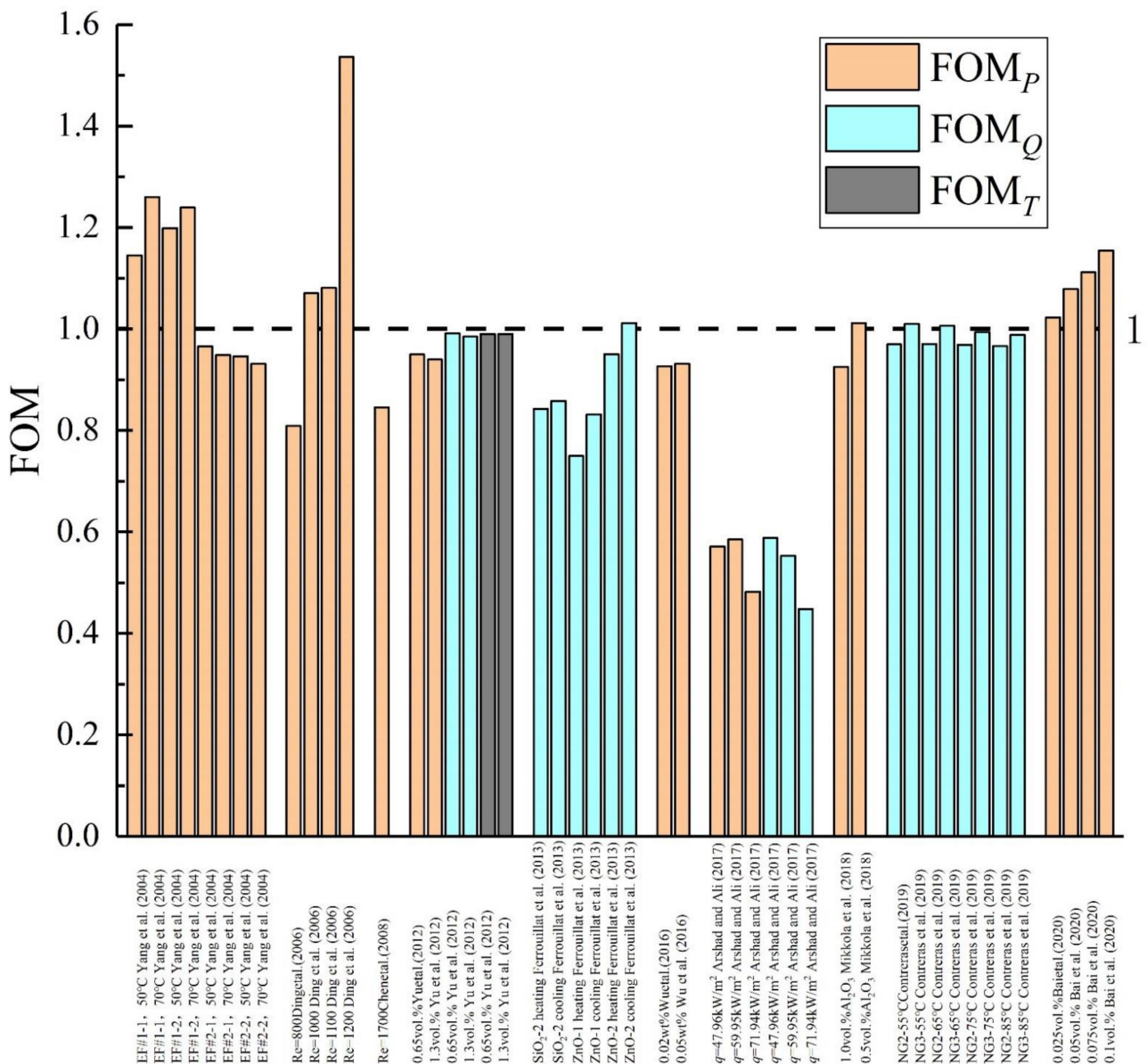


Figure 5. Thermohydraulic performance evaluation in the literature [3,10,23,42,100,101,103–105].

3.2. Numerical Predictions and Mechanism Discussion

Zahmatkesh et al. [12] recently reviewed nanoparticle shape effects in different flow regimes. They listed approximately 60 relevant publications and found no uniform conclusion on the effect of nanoparticle shape on CHT. The platelet-shaped nanoparticles caused the best CHT performance in the natural and forced convection regimes. Nonetheless, most of the works reported the optimum CHT for the blade-shaped nanoparticles in the mixed convection regime. More attention has been channeled to numerical predictions [89], and only one of these studies is based on experiments [95]. Some typical numerical studies for CHT of NSN nanofluids are listed chronologically in Table 4. Minea et al. [106] recently performed a benchmark study on nanofluid simulations. The main difference between thermal conductivity and CHT is the state of particle additives. Driven by the hydrodynamics and the inhomogeneous temperature field, the movement and distribution of particles will be inhomogeneous.

3.2.1. Particle Concentration Distribution and Interaction

Sonication promotes the uniform dispersion of nanoparticles in the base fluid during preparation. Nonetheless, there is no uniform standard for optimal ultrasonication duration for different types of nanofluids [13]. In addition, the uniform distribution of nanoparticles is overlooked by researchers. Lin et al. [107] simulated the particle number concentration in a straight pipe using the method of moments. The results revealed the non-uniformity of the cylindrical nanoparticle volume concentration across the section. Yuan et al. [108] modeled the Poiseuille flow and CHT of nanofluids in a circular minichannel and found that the nanorod volume fraction distribution is non-uniform near the boundary.

In contrast, the particles are more uniform when their aspect ratio is larger. The thermal resistance and temperature gradient are largest near the wall and are sensitive to particle concentration. Lin et al. [109–111] investigated the distribution and deposition of cylindrical nanoparticles in turbulent straight and curved pipes. The coupled model considered the effect of turbulent diffusivity on particle concentration distribution and interaction. The results revealed that the distribution of the particle concentration in the cross-section becomes non-uniform along the flow direction. In the curved duct, the extent of non-uniformity of the distribution of the particle number concentration increases with increasing Stokes number, Dean number, Reynolds number, and particle AR. They showed that particle transport and deposition in curved tubes are important; however, limited studies have considered the effect. Their numerical results demonstrated that the penetration efficiency increases as the Dean number, Reynolds number, and particle aspect ratio decrease. The penetration efficiency is highest when the Stokes number is approximately 0.02.

3.2.2. Particle Rotational Diffusion and Orientation Distribution

The morphology and orientation of the dispersed solids are complex in particle suspensions. Yu et al. [10] suggested four possible particle configurations in nanofluids, including the parallel series, Hashin–Shtrikman (or H-S), and EMT configurations. Researchers assume the H-S configuration when the TCE is estimated [64,72]. Nevertheless, the alignment of non-spherical nanoparticles is apparent in internal flows, specifically near the wall. Researchers give less consideration to the orientation distribution of nanoparticles. Elias et al. [112,113] found the highest overall heat transfer coefficient when nanofluids with cylindrical shapes were used for nanofluid flow in a shell and tube heat exchanger.

Moreover, non-spherical nanoparticles rotate, which delays and disturbs the thermal boundary layer [102]. The rotational diffusion coefficient of nanoparticles has recently attracted research attention. Lin et al. [109–111] and Yuan et al. [108] analyzed the turbulent and laminar NSN nanofluid flows in straight or turbulent pipes by considering the Brownian rotational diffusion and orientation distribution. They found that the orientation distribution of cylindrical nanoparticles was less concentrated as the Reynolds number increased in the turbulent regime. Particle orientation components at the cross-section are nearly $1/3$, implying that the nanorod orientation is nearly random in space at the channel center. The nanorod is more likely to align with the flow direction with the increasing shear near the wall. A nanorod with a higher aspect ratio is likely to be rotating towards the flow direction.

Table 4. Typical numerical studies for CHT of NSN nanofluids.

Authors	Nanofluid	Particle Shape and Size (nm)	Particle Loading	Flow State	CHT Enhancement
Elias et al. [112,113]	γ -AlOOH-EG and water (50/50)	Cylinder, AR = 1:8 Brick, AR = 1:1:1 Blade, AR = 1:6:1/12 Platelet, AR = 1:1/8	<1 vol.%	In shell and tube heat exchanger	Cylinder > brick > blade > platelet > sphere, for h , entropy generation, and heat transfer rate of nanofluid
Amin et al. [114]	Al ₂ O ₃ -water/Ethylene glycol	Blades, 1:6:1.12 Cylinders, AR = 8 Bricks, 1:1:1	1 vol.%	Flat-plate solar collector tube 12,000 < Re < 25,000	Brick-shape particles have the highest Nusselt number
Ooi and Popov [115]	Cu-water	Oblate spheroid, Prolate spheroid	<20 vol.%	Natural convection in a square cavity Marangoni boundary layer flow	Increases the CHT as well as flow resistance
Lin et al. [116]	Cu-water	Cube, rod, lamina, tetrahedron	<6 vol.%		Sphere nanoparticles have the best CHT enhancement
Lin et al. [107]	Al ₂ O ₃ -PAO	Cylinder AR = 6, 12, 18	0.65, 1.3, 2.5 vol.%	Laminar, 100 < Re < 2000	Nusselt number increases with ϕ , derived Nu formula based on the numerical data
Yuan et al. [117]	ZnO-water	Cylinder AR = 8, 12, 16	0.4, 0.93, 1.3 vol.%	Turbulent, 2500 < Re < 15,000	Nu _{nf} /Nu _f increases when Reynolds number, AR and ϕ grow
Trodi and Benhamza [118]	Al ₂ O ₃ -water	Oblate spheroid, $d_p = 1$ Prolate spheroid, $d_p = 2, 5, 7.5$ and 10	5, 10 vol.%	Flow in differentially heated square enclosures, 10 ³ < Ra < 10 ⁶	Heat transfer increases with Ra and ϕ , oblate spheroid has the best performance
Liu et al. [119]	Al ₂ O ₃ -water	Platelet, 78.6 (d) \times 9.8 (l) Blade, 85 (l) \times 14.15 (w) \times 1.18 (h) Cylinder, 19.6 (d) \times 157 (l) Brick, 36.6 (l) Platelets, AR = 0.125	0.5, 1, 1.5, 2 vol.%	Curved square duct laminar flow	Eulerian-Lagrangian two-phase approach
Sheikhzadeh and Aghaei [120]	Al ₂ O ₃ /SiO ₂ -water	Blades, 1:6:1.12 Cylinders, AR = 8 Bricks, 1:1:1	2-4 vol.%	Square cavity flow, 10 ⁵ < Ra < 10 ⁷	Platelets and cylindrical nanoparticles are more effective
Lin et al. [121]	ZnO-water	Cylinder AR = 2, 6, 10, 14	<5 vol.%	Curved pipe flow, 5000 \leq Re \leq 30,000	Nanofluid PEC is higher than base fluid PEC

4. Conclusions

Research on heat transfer enhancement of nanofluids is a long-term global initiative, and the unified understanding of this issue continues. Herein, we reviewed the heat transfer enhancement of nanofluids containing non-spherical nanoparticles. Non-spherical nanoparticles suspended in nanofluids were divided into three categories based on the dimension of the geometric particle structure. We collected and analyzed data on thermal conductivity and convective heat transfer enhancement of nanofluids measured in experiments. Recent studies investigated the numerical predictions and related heat transfer mechanisms. The main conclusions for NSN nanofluids are as follows:

Due to large aspect ratios, thermal conductivity is enhanced abnormally only for nanofluids containing carbon nanotubes/nanofibers/nanowires. On the other hand, thermal conductivity enhancement per concentration is larger for nanorods/ellipsoids with small aspect ratios. The enhancement of the network effect on heat transfer is limited. Polygonal particles enhanced the thermal conductivity least due to the sphericity being close to 1. The approximate enhancement effect by three types of non-spherical nanoparticles on thermal conductivity is 4.5:2.5:1. However, the particle size effect on nanofluids' thermal conductivity is unclear.

The convective heat transfer coefficient is increased by suspending non-spherical nanoparticles in the base fluid. Due to the increase in pumping power, no significant thermohydraulic performance was found for convective heat transfer of NSN nanofluid

flow. NSN nanofluid is uneconomical for turbulent flows, and the temperature and particle concentration effect on convective heat transfer remains unclear. In addition, there is no perfect model to precisely predict the thermal conductivity and convective heat transfer of NSN nanofluids.

Author Contributions: Conceptualization, X.L. and F.Y.; investigation, D.W.; resources, X.Y.; data curation, W.T.; writing—original draft preparation, C.D.; writing—review and editing, X.L.; visualization, J.D.; supervision, W.Y.; project administration, H.Y.; funding acquisition, F.Y. All authors have read and agreed to the published version of the manuscript.

Funding: This research was funded by the National Natural Science Foundation of China (No. 12172152, 11802105).

Institutional Review Board Statement: Not applicable.

Informed Consent Statement: Not applicable.

Data Availability Statement: Not applicable.

Conflicts of Interest: The authors declare no conflict of interest.

Abbreviations

NSN nanofluid	Nanofluid containing non-spherical nanoparticles
TCE	Thermal conductivity enhancement
CHT	Convective heat transfer
DW	Distilled water
CNTs	Carbon nanotubes
GNPs	Graphene nanoplatelets
AR	Aspect ratio
EG	Ethylene glycol
EHC	Effective heat conductivity
MD	Molecular dynamics
FOM	Figure of merit
PEC	Performance evaluation criteria
PAO	Polyalphaolefin
DFT	Density functional theory

Nomenclature

k	Thermal conductivity (W/(m·K))
Re	Reynolds number
Nu	Nusselt number
h	Convective heat transfer coefficient (W/(m ² ·K))
ϕ	Particle volume fraction
d	Particle diameter (nm)
l	Particle length (nm)
h	Particle length (nm)
P	Pumping power
Q	Flow rate
q	Heat flux (kW/m ²)
c_p	Specific heat capacity
ρ	Density (kg/m ³)
T_{s_i}	Temperature (K)sphericity

Subscripts

f	Base fluid
nfb	NanofluidBulk

References

- Choi, S.; Eastman, J. Enhancing thermal conductivity of fluids with nanoparticles. In Proceedings of the ASME International Mechanical Engineering Congress & Exposition, San Francisco, CA, USA, 12–17 November 1995; pp. 99–106.
- Murshed, S.M.S.; Leong, K.C.; Yang, C. Enhanced thermal conductivity of TiO₂—water based nanofluids. *Int. J. Therm. Sci.* **2005**, *44*, 367–373. [[CrossRef](#)]

3. Chen, H.; Yang, W.; He, Y.; Ding, Y.; Zhang, L.; Tan, C.; Lapkin, A.A.; Bavykin, D.V. Heat transfer and flow behaviour of aqueous suspensions of titanate nanotubes (nanofluids). *Powder Technol.* **2008**, *183*, 63–72. [[CrossRef](#)]
4. Chen, H.; Ding, Y.; Lapkin, A. Rheological behaviour of nanofluids containing tube/rod-like nanoparticles. *Powder Technol.* **2009**, *194*, 132–141. [[CrossRef](#)]
5. Murshed, S.M.S.; Estellé, P. A state of the art review on viscosity of nanofluids. *Renew. Sustain. Energy Rev.* **2017**, *76*, 1134–1152. [[CrossRef](#)]
6. Yu, W.; France, D.M.; Routbort, J.L.; Choi, S.U.S. Review and Comparison of Nanofluid Thermal Conductivity and Heat Transfer Enhancements. *Heat Transf. Eng.* **2008**, *29*, 432–460. [[CrossRef](#)]
7. Aybar, H.; Sharifpur, M.; Azizian, M.R.; Mehrabi, M.; Meyer, J.P. A Review of Thermal Conductivity Models for Nanofluids. *Heat Transf. Eng.* **2015**, *36*, 1085–1110. [[CrossRef](#)]
8. Murshed, S.S.; de Castro, C.N.; Lourenço, M.; Lopes, M.; Santos, F. A review of boiling and convective heat transfer with nanofluids. *Renew. Sustain. Energy Rev.* **2011**, *15*, 2342–2354. [[CrossRef](#)]
9. Hussein, A.M.; Sharma, K.; Bakar, R.; Kadirgama, K. A review of forced convection heat transfer enhancement and hydrodynamic characteristics of a nanofluid. *Renew. Sustain. Energy Rev.* **2014**, *29*, 734–743. [[CrossRef](#)]
10. Yu, L.; Liu, D.; Botz, F. Laminar Convective Heat Transfer of Alumina-Polyalphaolefin Nanofluids Containing Spherical and Non-Spherical Nanoparticles. In Proceedings of the International Electronic Packaging Technical Conference and Exhibition, Portland, OR, USA, 6–8 July 2011; Volume 44625, pp. 343–355. [[CrossRef](#)]
11. Yang, L.; Chen, X.; Xu, M.; Du, K. Roles of surfactants and particle shape in the enhanced thermal conductivity of TiO₂ nanofluids. *AIP Adv.* **2016**, *6*, 95104. [[CrossRef](#)]
12. Zahmatkesh, I.; Sheremet, M.; Yang, L.; Heris, S.Z.; Sharifpur, M.; Meyer, J.P.; Ghalambaz, M.; Wongwises, S.; Jing, D.; Mahian, O. Effect of nanoparticle shape on the performance of thermal systems utilizing nanofluids: A critical review. *J. Mol. Liq.* **2020**, *321*, 114430. [[CrossRef](#)]
13. Qiu, L.; Zhu, N.; Feng, Y.; Michaelides, E.E.; Żyła, G.; Jing, D.; Zhang, X.; Norris, P.M.; Markides, C.N.; Mahian, O. A review of recent advances in thermophysical properties at the nanoscale: From solid state to colloids. *Phys. Rep.* **2019**, *843*, 1–81. [[CrossRef](#)]
14. Bird, R.B.; Stewart, W.E.; Lightfoot, E.N. *Transport Phenomena*; John Wiley & Sons: New York, NY, USA, 2002.
15. Zhang, X.; Gu, H.; Fujii, M. Effective thermal conductivity and thermal diffusivity of nanofluids containing spherical and cylindrical nanoparticles. *Exp. Therm. Fluid Sci.* **2007**, *31*, 593–599. [[CrossRef](#)]
16. Cao, G.; Wang, Y. *Nanostructures and Nanomaterials: Synthesis, Properties and Applications*; World Scientific: London, UK, 2011.
17. Buschmann, M.; Azizian, R.; Kempe, T.; Juliá, J.E.; Martínez-Cuenca, R.; Sundén, B.; Wu, Z.; Seppälä, A.; Ala-Nissila, T. Correct interpretation of nanofluid convective heat transfer. *Int. J. Therm. Sci.* **2018**, *129*, 504–531. [[CrossRef](#)]
18. Mahian, O.; Kolsi, L.; Amani, M.; Estellé, P.; Ahmadi, G.; Kleinstreuer, C.; Marshall, J.S.; Siavashi, M.; Taylor, R.A.; Niazmand, H.; et al. Recent advances in modeling and simulation of nanofluid flows—Part I: Fundamentals and theory. *Phys. Rep.* **2018**, *790*, 1–48. [[CrossRef](#)]
19. Murshed, S.S.; de Castro, C.A.N. Superior thermal features of carbon nanotubes-based nanofluids—A review. *Renew. Sustain. Energy Rev.* **2014**, *37*, 155–167. [[CrossRef](#)]
20. Yazid, M.N.A.W.M.; Sidik, N.A.C.; Yahya, W.J. Heat and mass transfer characteristics of carbon nanotube nanofluids: A review. *Renew. Sustain. Energy Rev.* **2017**, *80*, 914–941. [[CrossRef](#)]
21. Ali, N.; Bahman, A.; Aljuwayhel, N.; Ebrahim, S.; Mukherjee, S.; Alsayegh, A. Carbon-Based Nanofluids and Their Advances towards Heat Transfer Applications—A Review. *Nanomaterials* **2021**, *11*, 1628. [[CrossRef](#)]
22. Xie, H.; Lee, H.; Youn, W.; Choi, M. Nanofluids containing multiwalled carbon nanotubes and their enhanced thermal conductivities. *J. Appl. Phys.* **2003**, *94*, 4967. [[CrossRef](#)]
23. Yang, Y.; Zhang, Z.G.; Grulke, E.A.; Anderson, W.B.; Wu, G. Heat transfer properties of nanoparticle-in-fluid dispersions (nanofluids) in laminar flow. *Int. J. Heat Mass Transf.* **2005**, *48*, 1107–1116. [[CrossRef](#)]
24. Gu, B.; Hou, B.; Lu, Z.; Wang, Z.; Chen, S. Thermal conductivity of nanofluids containing high aspect ratio fillers. *Int. J. Heat Mass Transf.* **2013**, *64*, 108–114. [[CrossRef](#)]
25. Maheshwary, P.; Handa, C.; Nemade, K.; Chaudhary, S. Role of nanoparticle shape in enhancing the thermal conductivity of nanofluids. *Mater. Today Proc.* **2020**, *28*, 873–878. [[CrossRef](#)]
26. Maheshwary, P.; Handa, C.; Nemade, K. A comprehensive study of effect of concentration, particle size and particle shape on thermal conductivity of titania/water based nanofluid. *Appl. Therm. Eng.* **2017**, *119*, 79–88. [[CrossRef](#)]
27. Zhu, D.; Wang, L.; Yu, W.; Xie, H. Intriguingly high thermal conductivity increment for CuO nanowires contained nanofluids with low viscosity. *Sci. Rep.* **2018**, *8*, 5282. [[CrossRef](#)]
28. Zhang, L.; Yu, W.; Zhu, D.; Xie, H.; Huang, G. Enhanced Thermal Conductivity for Nanofluids Containing Silver Nanowires with Different Shapes. *J. Nanomater.* **2017**, *2017*, 1–6. [[CrossRef](#)]
29. Carbajal-Valdez, R.; Rodríguez-Juárez, A.; Jiménez-Pérez, J.; Sánchez-Ramírez, J.; Cruz-Orea, A.; Correa-Pacheco, Z.; Macias, M.; Luna-Sánchez, J. Experimental investigation on thermal properties of Ag nanowire nanofluids at low concentrations. *Thermochim. Acta* **2018**, *671*, 83–88. [[CrossRef](#)]
30. Xie, H.; Wang, J.; Xi, T.; Liu, Y. Thermal Conductivity of Suspensions Containing Nanosized SiC Particles. *Int. J. Thermophys.* **2002**, *23*, 571–580. [[CrossRef](#)]

31. Yang, B.; Han, Z.H. Temperature-dependent thermal conductivity of nanorod-based nanofluids. *Appl. Phys. Lett.* **2006**, *89*, 83111. [[CrossRef](#)]
32. Becker, J.; Trügler, A.; Jakab, A.; Hohenester, U.; Sönnichsen, C. The Optimal Aspect Ratio of Gold Nanorods for Plasmonic Bio-sensing. *Plasmonics* **2010**, *5*, 161–167. [[CrossRef](#)]
33. Zhu, H.T.; Zhang, C.Y.; Tang, A.Y.M.; Wang, J.X. Novel Synthesis and Thermal Conductivity of CuO Nanofluid. *J. Phys. Chem. C* **2007**, *111*, 1646–1650. [[CrossRef](#)]
34. Timofeeva, E.V.; Routbort, J.L.; Singh, D. Particle shape effects on thermophysical properties of alumina nanofluids. *J. Appl. Phys.* **2009**, *106*, 14304. [[CrossRef](#)]
35. Cui, W.; Cao, Z.; Li, X.; Lu, L.; Ma, T.; Wang, Q. Experimental investigation and artificial intelligent estimation of thermal conductivity of nanofluids with different nanoparticles shapes. *Powder Technol.* **2021**, *398*, 117078. [[CrossRef](#)]
36. Nithyanantham, U.; González-Fernández, L.; Grosu, Y.; Zaki, A.; Igartua, J.M.; Faik, A. Shape effect of Al₂O₃ nanoparticles on the thermophysical properties and viscosity of molten salt nanofluids for TES application at CSP plants. *Appl. Therm. Eng.* **2020**, *169*, 114942. [[CrossRef](#)]
37. Jiang, W.; Ding, G.; Peng, H. Measurement and model on thermal conductivities of carbon nanotube nanorefrigerants. *Int. J. Therm. Sci.* **2009**, *48*, 1108–1115. [[CrossRef](#)]
38. Singh, D.J.; Timofeeva, E.V.; Yu, W.; Routbort, J.L.; France, D.M.; Smith, D.Y.; Lopez-Cepero, J.M. An investigation of silicon carbide-water nanofluid for heat transfer applications. *J. Appl. Phys.* **2009**, *105*, 64306. [[CrossRef](#)]
39. Kim, H.J.; Lee, S.-H.; Lee, J.-H.; Jang, S.P. Effect of particle shape on suspension stability and thermal conductivities of water-based bohemite alumina nanofluids. *Energy* **2015**, *90*, 1290–1297. [[CrossRef](#)]
40. Torii, S.; Yang, W.-J. Heat Transfer Augmentation of Aqueous Suspensions of Nanodiamonds in Turbulent Pipe Flow. *J. Heat Transf.* **2009**, *131*, 43203. [[CrossRef](#)]
41. Xie, H.; Yu, W.; Li, Y. Thermal performance enhancement in nanofluids containing diamond nanoparticles. *J. Phys. D: Appl. Phys.* **2009**, *42*, 95413. [[CrossRef](#)]
42. Ferrouillat, S.; Bontemps, A.; Poncelet, O.; Soriano, O.; Gruss, J.-A. Influence of nanoparticle shape factor on convective heat transfer and energetic performance of water-based SiO₂ and ZnO nanofluids. *Appl. Therm. Eng.* **2013**, *51*, 839–851. [[CrossRef](#)]
43. Yang, L.; Ji, W.; Huang, J.-N.; Xu, G. An updated review on the influential parameters on thermal conductivity of nano-fluids. *J. Mol. Liq.* **2019**, *296*, 111780. [[CrossRef](#)]
44. Tahmooressi, H.; Kasaeian, A.; Yavarinasab, A.; Tarokh, A.; Ghazi, M.; Hoorfar, M. Numerical simulation of nanoparticles size/aspect ratio effect on thermal conductivity of nanofluids using lattice Boltzmann method. *Int. Commun. Heat Mass Transf.* **2020**, *120*, 105033. [[CrossRef](#)]
45. Assael, M.J.; Chen, C.-F.; Metaxa, I.; Wakeham, W.A. Thermal Conductivity of Suspensions of Carbon Nanotubes in Water. *Int. J. Thermophys.* **2004**, *25*, 971–985. [[CrossRef](#)]
46. Nasiri, A.; Shariaty-Niasar, M.; Rashidi, A.; Khodafarin, R. Effect of CNT structures on thermal conductivity and stability of nanofluid. *Int. J. Heat Mass Transf.* **2012**, *55*, 1529–1535. [[CrossRef](#)]
47. Fang, X.; Ding, Q.; Fan, L.-W.; Yu, Z.-T.; Xu, X.; Cheng, G.-H.; Hu, Y.-C.; Cen, K.-F. Thermal Conductivity Enhancement of Ethylene Glycol-Based Suspensions in the Presence of Silver Nanoparticles of Various Shapes. *J. Heat Transf.* **2013**, *136*, 34501. [[CrossRef](#)]
48. Jeong, J.; Li, C.; Kwon, Y.; Lee, J.; Kim, S.H.; Yun, R. Particle shape effect on the viscosity and thermal conductivity of ZnO nanofluids. *Int. J. Refrig.* **2013**, *36*, 2233–2241. [[CrossRef](#)]
49. Farbod, M.; Asl, R.K.; Abadi, A.R.N. Morphology dependence of thermal and rheological properties of oil-based nanofluids of CuO nanostructures. *Colloids Surfaces A Physicochem. Eng. Asp.* **2015**, *474*, 71–75. [[CrossRef](#)]
50. Shah, J.; Kumar, S.; Ranjan, M.; Sonvane, Y.; Thareja, P.; Gupta, S.K. The effect of filler geometry on thermo-optical and rheological properties of CuO nanofluid. *J. Mol. Liq.* **2018**, *272*, 668–675. [[CrossRef](#)]
51. Ni, Z.; Cao, X.; Wang, X.; Zhou, S.; Zhang, C.; Xu, B.; Ni, Y. Facile Synthesis of Copper(I) Oxide Nanochains and the Photo-Thermal Conversion Performance of Its Nanofluids. *Coatings* **2021**, *11*, 749. [[CrossRef](#)]
52. Maxwell, J.C. *A Treatise on Electricity and Magnetism*; Clarendon Press: London, UK, 1881; Volume 1.
53. Hamilton, R.L.; Crosser, O.K. Thermal Conductivity of Heterogeneous Two-Component Systems. *Ind. Eng. Chem. Fundam.* **1962**, *1*, 187–191. [[CrossRef](#)]
54. Wang, B.-X.; Zhou, L.-P.; Peng, X.-F. A fractal model for predicting the effective thermal conductivity of liquid with suspension of nanoparticles. *Int. J. Heat Mass Transf.* **2003**, *46*, 2665–2672. [[CrossRef](#)]
55. Hasselman, D.; Johnson, L.F. Effective Thermal Conductivity of Composites with Interfacial Thermal Barrier Resistance. *J. Compos. Mater.* **1987**, *21*, 508–515. [[CrossRef](#)]
56. Xue, L.; Keblinski, P.; Phillpot, S.; Choi, S.-S.; Eastman, J. Effect of liquid layering at the liquid–solid interface on thermal transport. *Int. J. Heat Mass Transf.* **2004**, *47*, 4277–4284. [[CrossRef](#)]
57. Nan, C.-W.; Liu, G.; Lin, Y.; Li, M. Interface effect on thermal conductivity of carbon nanotube composites. *Appl. Phys. Lett.* **2004**, *85*, 3549–3551. [[CrossRef](#)]
58. Zhou, X.F.; Gao, L. Effective thermal conductivity in nanofluids of nonspherical particles with interfacial thermal resistance: Differential effective medium theory. *J. Appl. Phys.* **2006**, *100*, 24913. [[CrossRef](#)]

59. Murshed, S.M.S.; Leong, K.; Yang, C. Investigations of thermal conductivity and viscosity of nanofluids. *Int. J. Therm. Sci.* **2008**, *47*, 560–568. [\[CrossRef\]](#)
60. Jiang, H.; Xu, Q.; Huang, C.; Shi, L. The role of interfacial nanolayer in the enhanced thermal conductivity of carbon nanotube-based nanofluids. *Appl. Phys. A* **2014**, *118*, 197–205. [\[CrossRef\]](#)
61. Chandrasekar, M.; Suresh, S.; Srinivasan, R.; Bose, A.C. New Analytical Models to Investigate Thermal Conductivity of Nanofluids. *J. Nanosci. Nanotechnol.* **2009**, *9*, 533–538. [\[CrossRef\]](#)
62. Yang, L.; Xu, X.; Jiang, W.; Du, K. A new thermal conductivity model for nanorod-based nanofluids. *Appl. Therm. Eng.* **2017**, *114*, 287–299. [\[CrossRef\]](#)
63. Yang, L.; Xu, X. A renovated Hamilton–Crosser model for the effective thermal conductivity of CNTs nanofluids. *Int. Commun. Heat Mass Transf.* **2016**, *81*, 42–50. [\[CrossRef\]](#)
64. Yang, L.; Du, K.; Zhang, X. A theoretical investigation of thermal conductivity of nanofluids with particles in cylindrical shape by anisotropy analysis. *Powder Technol.* **2016**, *314*, 328–338. [\[CrossRef\]](#)
65. Khalifeh, A.; Vaferi, B. Intelligent assessment of effect of aggregation on thermal conductivity of nanofluids—Comparison by experimental data and empirical correlations. *Thermochim. Acta* **2019**, *681*, 178377. [\[CrossRef\]](#)
66. Alawi, O.A.; Sidik, N.A.C.; Xian, H.W.; Kean, T.H.; Kazi, S. Thermal conductivity and viscosity models of metallic oxides nanofluids. *Int. J. Heat Mass Transf.* **2018**, *116*, 1314–1325. [\[CrossRef\]](#)
67. Wang, R.; Qian, S.; Zhang, Z. Investigation of the aggregation morphology of nanoparticle on the thermal conductivity of nanofluid by molecular dynamics simulations. *Int. J. Heat Mass Transf.* **2018**, *127*, 1138–1146. [\[CrossRef\]](#)
68. Chen, R.; Zhang, T.; Guo, Y.; Wang, J.; Wei, J.; Yu, Q. Recent advances in simultaneous removal of SO₂ and NO_x from exhaust gases: Removal process, mechanism and kinetics. *Chem. Eng. J.* **2020**, *420*, 127588. [\[CrossRef\]](#)
69. Du, J.; Su, Q.; Li, L.; Wang, R.; Zhu, Z. Evaluation of the influence of aggregation morphology on thermal conductivity of nanofluid by a new MPCD-MD hybrid method. *Int. Commun. Heat Mass Transf.* **2021**, *127*, 105501. [\[CrossRef\]](#)
70. Lee, J.W.; Nilson, R.H.; Templeton, J.A.; Griffiths, S.K.; Kung, A.; Wong, B.M. Comparison of Molecular Dynamics with Classical Density Functional and Poisson–Boltzmann Theories of the Electric Double Layer in Nanochannels. *J. Chem. Theory Comput.* **2012**, *8*, 2012–2022. [\[CrossRef\]](#)
71. Sastry, N.N.V.; Bhunia, A.; Sundararajan, T.; Das, S.K. Predicting the effective thermal conductivity of carbon nanotube based nanofluids. *Nanotechnology* **2008**, *19*, 55704. [\[CrossRef\]](#)
72. Koo, J.; Kang, Y.; Kleinstreuer, C. A nonlinear effective thermal conductivity model for carbon nanotube and nanofiber suspensions. *Nanotechnology* **2008**, *19*, 375705. [\[CrossRef\]](#)
73. Xue, Q.Z. Model for thermal conductivity of carbon nanotube-based composites. *Phys. B Condens. Matter* **2005**, *368*, 302–307. [\[CrossRef\]](#)
74. Sabbaghzadeh, J.; Ebrahimi, S. Effective Thermal Conductivity of Nanofluids Containing Cylindrical Nanoparticles. *Int. J. Nanosci.* **2007**, *6*, 45–49. [\[CrossRef\]](#)
75. Ebrahimi, S.; Sabbaghzadeh, J.; Lajevardi, M.; Hadi, I. Cooling performance of a microchannel heat sink with nanofluids containing cylindrical nanoparticles (carbon nanotubes). *Heat Mass Transf.* **2010**, *46*, 549–553. [\[CrossRef\]](#)
76. Yang, B. Thermal Conductivity Equations Based on Brownian Motion in Suspensions of Nanoparticles (Nanofluids). *J. Heat Transf.* **2008**, *130*, 42408. [\[CrossRef\]](#)
77. Koo, J.; Kleinstreuer, C. Impact analysis of nanoparticle motion mechanisms on the thermal conductivity of nanofluids. *Int. Commun. Heat Mass Transf.* **2005**, *32*, 1111–1118. [\[CrossRef\]](#)
78. Cui, W.; Bai, M.; Lv, J.; Li, G.; Li, X. On the Influencing Factors and Strengthening Mechanism for Thermal Conductivity of Nanofluids by Molecular Dynamics Simulation. *Ind. Eng. Chem. Res.* **2011**, *50*, 13568–13575. [\[CrossRef\]](#)
79. Yamada, E.; Ota, T. Effective thermal conductivity of dispersed materials. *Wärme-Und Stoffübertragung* **1980**, *13*, 27–37. [\[CrossRef\]](#)
80. Liang, G.; Mudawar, I. Review of pool boiling enhancement with additives and nanofluids. *Int. J. Heat Mass Transf.* **2018**, *124*, 423–453. [\[CrossRef\]](#)
81. Kamel, M.S.; Lezsovits, F. Boiling heat transfer of nanofluids: A review of recent studies. *Therm. Sci.* **2019**, *23*, 109–124. [\[CrossRef\]](#)
82. Barber, J.; Brutin, D.; Tadrist, L. A review on boiling heat transfer enhancement with nanofluids. *Nanoscale Res. Lett.* **2011**, *6*, 280. [\[CrossRef\]](#)
83. Vallejo, J.P.; Prado, J.I.; Lugo, L. Hybrid or mono nanofluids for convective heat transfer applications. A critical review of experimental research. *Appl. Therm. Eng.* **2021**, *203*, 117926. [\[CrossRef\]](#)
84. Al-Hossainy, A.; Eid, M.R. Structure, DFT calculations and heat transfer enhancement in [ZnO/PG + H₂O]C hybrid nanofluid flow as a potential solar cell coolant application in a double-tube. *J. Mater. Sci. Mater. Electron.* **2020**, *31*, 15243–15257. [\[CrossRef\]](#)
85. Alam, M.; Hussain, S.; Souayeh, B.; Khan, M.; Farhan, M. Numerical Simulation of Homogeneous–Heterogeneous Reactions through a Hybrid Nanofluid Flowing over a Rotating Disc for Solar Heating Applications. *Sustainability* **2021**, *13*, 8289. [\[CrossRef\]](#)
86. Hussain, S.; Pour, M.; Jamal, M.; Armaghani, T. MHD Mixed Convection and Entropy Analysis of Non-Newtonian Hybrid Nanofluid in a Novel Wavy Elbow-Shaped Cavity with a Quarter Circle Hot Block and a Rotating Cylinder. *Exp. Technol.* **2022**, *46*, 1–20. [\[CrossRef\]](#)
87. Khodabandeh, E.; Akbari, O.A.; Toghraie, D.; Pour, M.S.; Jönsson, P.G.; Ersson, M. Numerical investigation of thermal performance augmentation of nanofluid flow in microchannel heat sinks by using of novel nozzle structure: Sinusoidal cavities and rectangular ribs. *J. Braz. Soc. Mech. Sci. Eng.* **2019**, *41*, 443. [\[CrossRef\]](#)

88. Souayeh, B.; Bhattacharyya, S.; Hdhiri, N.; Alam, M.W.; Yasin, E.; Aamir, M. Investigation on inlet obstruction in transitional flow regime: Heat transfer augmentation and pressure drop analysis. *Case Stud. Therm. Eng.* **2022**, *34*, 102016. [[CrossRef](#)]
89. Ghasemiasl, R.; Hashemi, S.; Armaghani, T.; Tayebi, T.; Pour, M.S. Recent Studies on the Forced Convection of Nano-Fluids in Channels and Tubes: A Comprehensive Review. *Exp. Technol.* **2022**, *46*, 1–35. [[CrossRef](#)]
90. Wu, Z.; Wang, L.; Sundén, B. Pressure drop and convective heat transfer of water and nanofluids in a double-pipe helical heat exchanger. *Appl. Therm. Eng.* **2013**, *60*, 266–274. [[CrossRef](#)]
91. Buongiorno, J. Convective Transport in Nanofluids. *J. Heat Transfer.* **2006**, *128*, 240–250. [[CrossRef](#)]
92. Myers, T.G.; Ribera, H.; Cregan, V. Does mathematics contribute to the nanofluid debate? *Int. J. Heat Mass Transf.* **2017**, *111*, 279–288. [[CrossRef](#)]
93. Yu, L.; Liu, N. Study of the Thermal Effectiveness of Laminar Forced Convection of Nanofluids for Liquid Cooling Applications. *IEEE Trans. Compon. Packag. Manuf. Technol.* **2013**, *3*, 1693–1704. [[CrossRef](#)]
94. Alkasmoul, F.S.; Al-Asadi, M.; Myers, T.; Thompson, H.; Wilson, M. A practical evaluation of the performance of Al₂O₃-water, TiO₂-water and CuO-water nanofluids for convective cooling. *Int. J. Heat Mass Transf.* **2018**, *126*, 639–651. [[CrossRef](#)]
95. Paul, T.C.; Morshed, A.; Fox, E.; Khan, J.A. Experimental investigation of natural convection heat transfer of Al₂O₃ Nanoparticle Enhanced Ionic Liquids (NEILs). *Int. J. Heat Mass Transf.* **2015**, *83*, 753–761. [[CrossRef](#)]
96. Ji, Y.; Wilson, C.; Chen, H.-H.; Ma, H. Particle shape effect on heat transfer performance in an oscillating heat pipe. *Nanoscale Res. Lett.* **2011**, *6*, 296. [[CrossRef](#)] [[PubMed](#)]
97. Nelson, I.C.; Banerjee, D.; Ponnappan, R. Flow Loop Experiments Using Polyalphaolefin Nanofluids. *J. Thermophys. Heat Transf.* **2009**, *23*, 752–761. [[CrossRef](#)]
98. Ben Mansour, R.; Galanis, N.; Nguyen, C.T. Effect of uncertainties in physical properties on forced convection heat transfer with nanofluids. *Appl. Therm. Eng.* **2007**, *27*, 240–249. [[CrossRef](#)]
99. Ali, H.M.; Arshad, W. Effect of channel angle of pin-fin heat sink on heat transfer performance using water based graphene nanoplatelets nanofluids. *Int. J. Heat Mass Transf.* **2017**, *106*, 465–472. [[CrossRef](#)]
100. Arshad, W.; Ali, H.M. Graphene nanoplatelets nanofluids thermal and hydrodynamic performance on integral fin heat sink. *Int. J. Heat Mass Transf.* **2017**, *107*, 995–1001. [[CrossRef](#)]
101. Mikkola, V.; Puupponen, S.; Granbohm, H.; Saari, K.; Ala-Nissila, T.; Seppälä, A. Influence of particle properties on convective heat transfer of nanofluids. *Int. J. Therm. Sci.* **2018**, *124*, 187–195. [[CrossRef](#)]
102. Wu, Z.; Wang, L.; Sundén, B.; Wadsö, L. Aqueous carbon nanotube nanofluids and their thermal performance in a helical heat exchanger. *Appl. Therm. Eng.* **2016**, *96*, 364–371. [[CrossRef](#)]
103. Contreras, E.M.C.; Oliveira, G.A.; Filho, E.B. Experimental analysis of the thermohydraulic performance of graphene and silver nanofluids in automotive cooling systems. *Int. J. Heat Mass Transf.* **2019**, *132*, 375–387. [[CrossRef](#)]
104. Bai, M.-J.; Liu, J.-L.; He, J.; Li, W.-J.; Wei, J.-J.; Chen, L.-X.; Miao, J.-Y.; Li, C.-M. Heat transfer and mechanical friction reduction properties of graphene oxide nanofluids. *Diam. Relat. Mater.* **2020**, *108*, 107982. [[CrossRef](#)]
105. Ding, Y.; Alias, H.; Wen, D.; Williams, R.A. Heat transfer of aqueous suspensions of carbon nanotubes (CNT nanofluids). *Int. J. Heat Mass Transf.* **2006**, *49*, 240–250. [[CrossRef](#)]
106. Minea, A.A.; Buonomo, B.; Burggraf, J.; Ercole, D.; Karpaiya, K.R.; Di Pasqua, A.; Sekrani, G.; Steffens, J.; Tibaut, J.; Wichmann, N.; et al. NanoRound: A benchmark study on the numerical approach in nanofluids' simulation. *Int. Commun. Heat Mass Transf.* **2019**, *108*, 104292. [[CrossRef](#)]
107. Lin, J.; Xia, Y.; Ku, X. Friction factor and heat transfer of nanofluids containing cylindrical nanoparticles in laminar pipe flow. *J. Appl. Phys.* **2014**, *116*, 133513. [[CrossRef](#)]
108. Yuan, F.; Yu, W.; Lin, J. Numerical study of the effects of nanorod aspect ratio on Poiseuille flow and convective heat transfer in a circular minichannel. *Microfluid. Nanofluidics* **2020**, *24*, 1–15. [[CrossRef](#)]
109. Lin, J.; Shi, R.; Yuan, F.; Yu, M. Distribution and penetration efficiency of cylindrical nanoparticles in turbulent flows through a curved tube. *Aerosol Sci. Technol.* **2020**, *54*, 1255–1269. [[CrossRef](#)]
110. Lin, W.; Shi, R.; Lin, J. Distribution and Deposition of Cylindrical Nanoparticles in a Turbulent Pipe Flow. *Appl. Sci.* **2021**, *11*, 962. [[CrossRef](#)]
111. Lin, J.-Z.; Xia, Y.; Ku, X.-K. Flow and heat transfer characteristics of nanofluids containing rod-like particles in a turbulent pipe flow. *Int. J. Heat Mass Transf.* **2016**, *93*, 57–66. [[CrossRef](#)]
112. Elias, M.; Miqdad, M.; Mahbulul, I.; Saidur, R.; Kamalisarvestani, M.; Sohel, M.; Hepbasli, A.; Rahim, N.; Amalina, M. Effect of nanoparticle shape on the heat transfer and thermodynamic performance of a shell and tube heat exchanger. *Int. Commun. Heat Mass Transf.* **2013**, *44*, 93–99. [[CrossRef](#)]
113. Elias, M.; Shahrul, I.; Mahbulul, I.; Saidur, R.; Rahim, N. Effect of different nanoparticle shapes on shell and tube heat exchanger using different baffle angles and operated with nanofluid. *Int. J. Heat Mass Transf.* **2014**, *70*, 289–297. [[CrossRef](#)]
114. Amin, T.E.; Roghayeh, G.; Fatemeh, R.; Fatollah, P. Evaluation of Nanoparticle Shape Effect on a Nanofluid Based Flat-Plate Solar Collector Efficiency. *Energy Explor. Exploit.* **2015**, *33*, 659–676. [[CrossRef](#)]
115. Ooi, E.H.; Popov, V. Numerical study of influence of nanoparticle shape on the natural convection in Cu-water nanofluid. *Int. J. Therm. Sci.* **2013**, *65*, 178–188. [[CrossRef](#)]
116. Lin, Y.; Li, B.; Zheng, L.; Chen, G. Particle shape and radiation effects on Marangoni boundary layer flow and heat transfer of copper-water nanofluid driven by an exponential temperature. *Powder Technol.* **2016**, *301*, 379–386. [[CrossRef](#)]

117. Yuan, F.; Lin, J.; Ku, X. Convective Heat Transfer and Resistance Characteristics of Nanofluids with Cylindrical Particles. *Heat Transf. Eng.* **2017**, *39*, 526–535. [[CrossRef](#)]
118. Trodi, A.; Benhamza, M.E.H. Particle Shape and Aspect Ratio Effect of Al₂O₃–Water Nanofluid on Natural Convective Heat Transfer Enhancement in Differentially Heated Square Enclosures. *Chem. Eng. Commun.* **2016**, *204*, 158–167. [[CrossRef](#)]
119. Liu, F.; Cai, Y.; Wang, L.; Zhao, J. Effects of nanoparticle shapes on laminar forced convective heat transfer in curved ducts using two-phase model. *Int. J. Heat Mass Transf.* **2017**, *116*, 292–305. [[CrossRef](#)]
120. Sheikhzadeh, G.A.; Aghaei, A.; Soleimani, S. Effect of nanoparticle shape on natural convection heat transfer in a square cavity with partitions using water-SiO₂ nanofluid. *Chall. Nano Micro Scale Sci. Technol.* **2018**, *6*, 27–38. [[CrossRef](#)]
121. Lin, W.; Shi, R.; Lin, J. Heat Transfer and Pressure Drop of Nanofluid with Rod-like Particles in Turbulent Flows through a Curved Pipe. *Entropy* **2022**, *24*, 416. [[CrossRef](#)]